nature portfolio

https://doi.org/10.1038/s41557-020-00614-w

Supplementary information

Iron-catalysed synthesis and chemical recycling of telechelic 1,3-enchained oligocyclobutanes

In the format provided by the authors and unedited

Supplementary Information

Iron-Catalyzed Synthesis and Chemical Recycling of Telechelic 1,3-Enchained Oligocyclobutanes

*Megan Mohadjer Beromi, C. Rose Kennedy, Jarod M. Younker, Alex E. Carpenter, Sarah J. Mattler, Joseph A. Throckmorton, and Paul J. Chirik**

Department of Chemistry, Frick Laboratory
Princeton University, Princeton, NJ 08544, USA

ExxonMobil Chemical Company, Baytown, TX 77520, USA

pchirik@princeton.edu

Table of Contents

I. Spectroscopic Data for Oligocyclobutanes

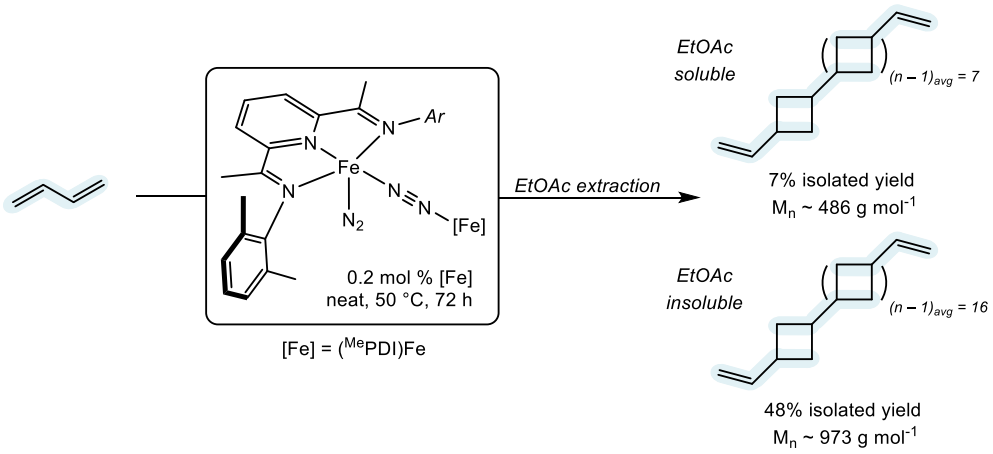

Spectroscopic Data for (1,n')-divinyl-oligocyclobutane:

Spectroscopic data for ethyl acetate soluble fraction: ^{1}H NMR (500 MHz, chloroform-*d*, 25 ºC): δ 6.04-5.96 (m, 1H), 5.91-5.83 (m, 1H), 4.96-4.86 (m, 4H), 2.83 (app. p, *J* = 6.4 Hz, 1H), 2.71 (app. p, *J* = 7.7 Hz, 1H), 2.28-1.78 (m, 27H), 1.69-1.56 (m, 10H), 1.46-1.40 (m, 3H), 1.25-1.17 (m, 8H). The ^{1}H NMR spectrum is given in Figure 1A. ^{13}C{^{1}H} NMR (500 MHz, chloroform-*d*, 25 ºC): δ 143.89, 143.61, 112.02, 111.75, 36.74, 36.71, 36.63, 36.52, 36.49, 36.31, 36.26, 36.14, 36.08, 36.04, 35.98, 35.96, 35.86, 35.73, 35.63, 35.10, 34.81, 34.63, 34.54, 31.83, 31.41, 30.78, 30.42, 29.25, 29.14, 28.83, 28.75, 28.73, 28.68, 28.59, 28.54, 28.31, 28.28, 28.25, 28.19, 28.13, 28.04, 27.71, 27.63. The ^{13}C NMR spectrum is given in Figure 1B.

Spectroscopic data for ethyl acetate insoluble fraction: ^{1}H NMR (400 MHz, 1,1,2,2-tetrachloroethane-d_2, 120 ºC): δ 6.14-6.06 (m, 1H), 5.97-5.91 (obs. m, 1H), 5.05-4.93 (m, 4H), 2.94-2.87 (app. p, *J* = 6.5 Hz, 1H), 2.81-2.74 (app. p, *J* = 7.5 Hz, 1H), 2.51-1.86 (m, 52 H), 1.77-1.70 (m, 20H), 1.57-1.50 (m, 4H), 1.43-1.25 (m, 20H), 1.12-0.81 (m, 2H). The ^{1}H NMR spectrum is given in Figure 2A. ^{13}C{^{1}H} NMR (400 MHz, 1,1,2,2-tetrachloroethane-d_2, 120 ºC): δ 143.56, 143.25, 111.54, 111.33, 36.57, 36.56, 36.53, 36.51, 36.49, 36.47, 36.46, 36.27, 36.06, 36.02, 36.00, 35.95, 35.94, 35.81, 35.77, 35.73, 35.71, 35.69, 35.59, 34.51, 34.26, 34.16, 34.08, 31.63, 31.61, 31.35, 30.64, 30.62, 30.37, 30.35, 29.37, 28.97, 28.95, 28.70, 28.65, 28.57, 28.38, 28.33,

28.31, 28.25, 28.17, 27.87, 27.57. Multiple signals were not resolved. The ^{13}C NMR spectrum is given in Figure 2B.

The ethyl acetate soluble material was also analyzed by $^{13}C\{^{1}H\}$ APT, COSY, HSQC, HMBC, NOESY, and TOCSY NMR spectroscopy to validate the proposed structure of the oligomer. The spectra and assignments are given in Figures 3A-F.

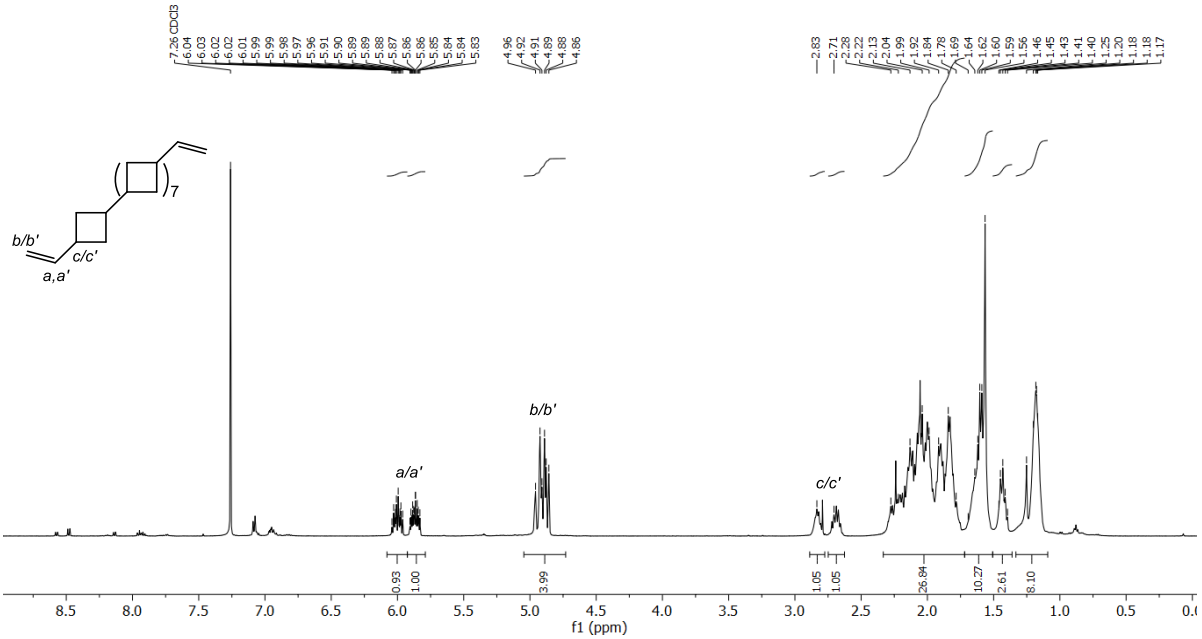

Figure 1A. ^{1}H NMR (500 MHz, chloroform-*d*, 25 ºC) spectrum of (1,n'-divinyl)oligocyclobutane (M_n ~ 486 g mol^{-1}, 8 cyclobutyls). Chain end assignments are given.

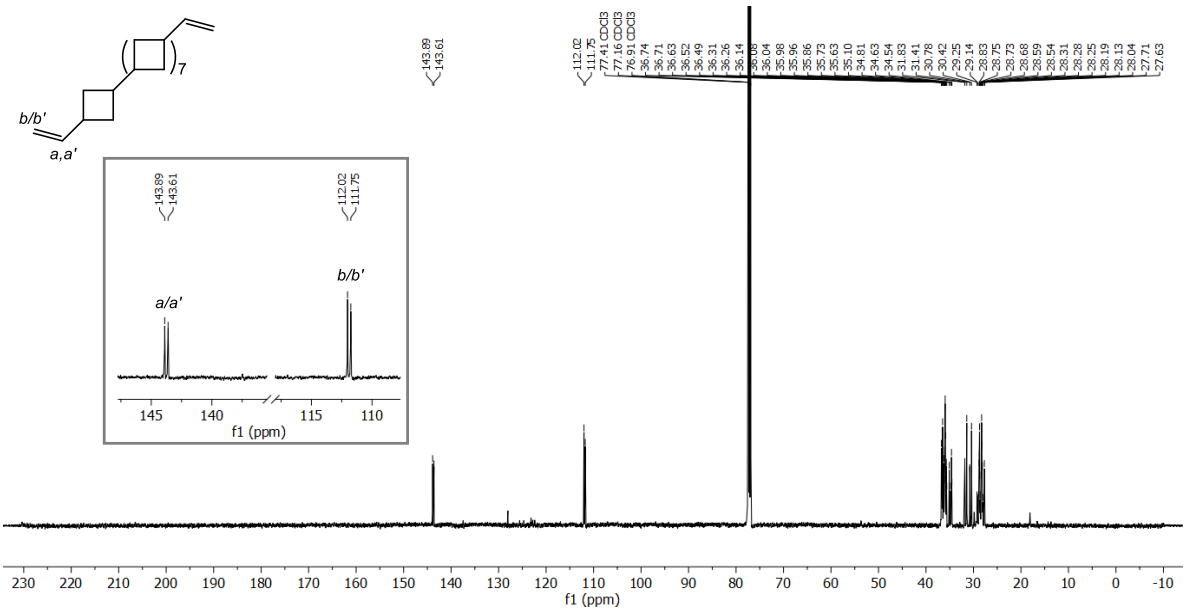

Figure 1B. ^{13}C{^{1}H} NMR (126 MHz, chloroform-*d*, 25 ºC) spectrum of (1,n'-divinyl)oligocyclobutane (M_n ~ 486 g mol^{-1}, 8 cyclobutyls). Inset: Expansion of region containing resonances corresponding to chain end diastereomers. Chain end assignments are given.

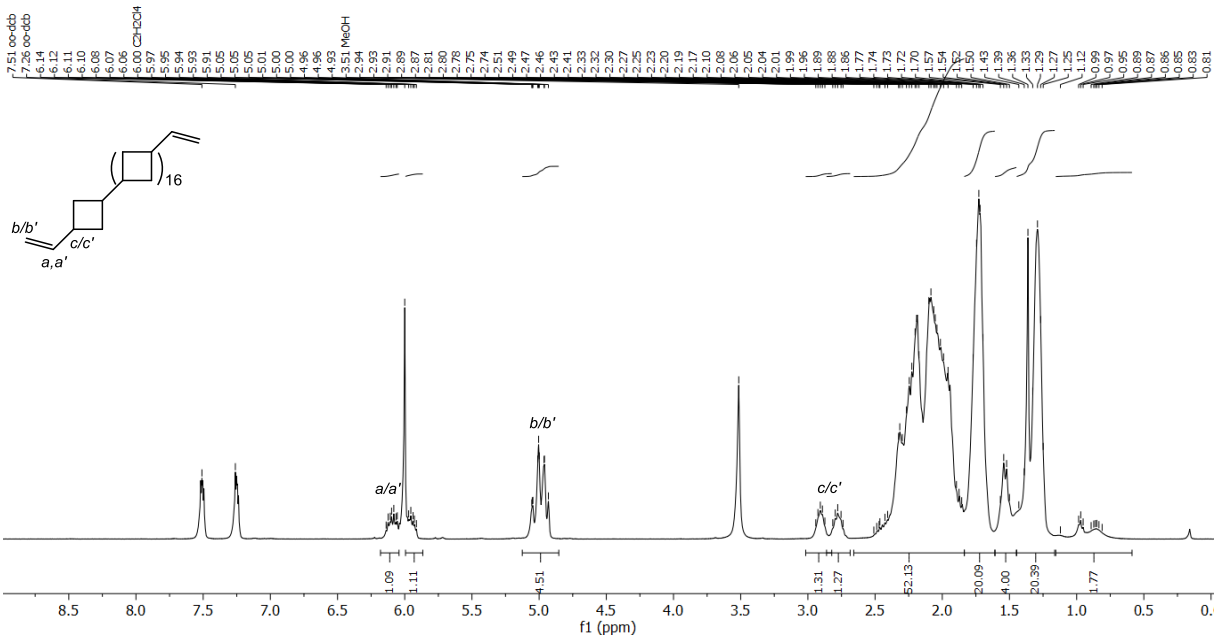

Figure 2A. ^{1}H NMR (400 MHz, 1,1,2,2-tetrachloroethane-d_2, 120 ºC) spectrum of (1,n'-divinyl)oligocyclobutane (M_n ~ 973 g mol^{-1}, 17 cyclobutyls). Chain end assignments are given. Residual *o,o*-dichlorobenzene (o,o-dcb) and methanol (MeOH) from purification are present in the spectrum.

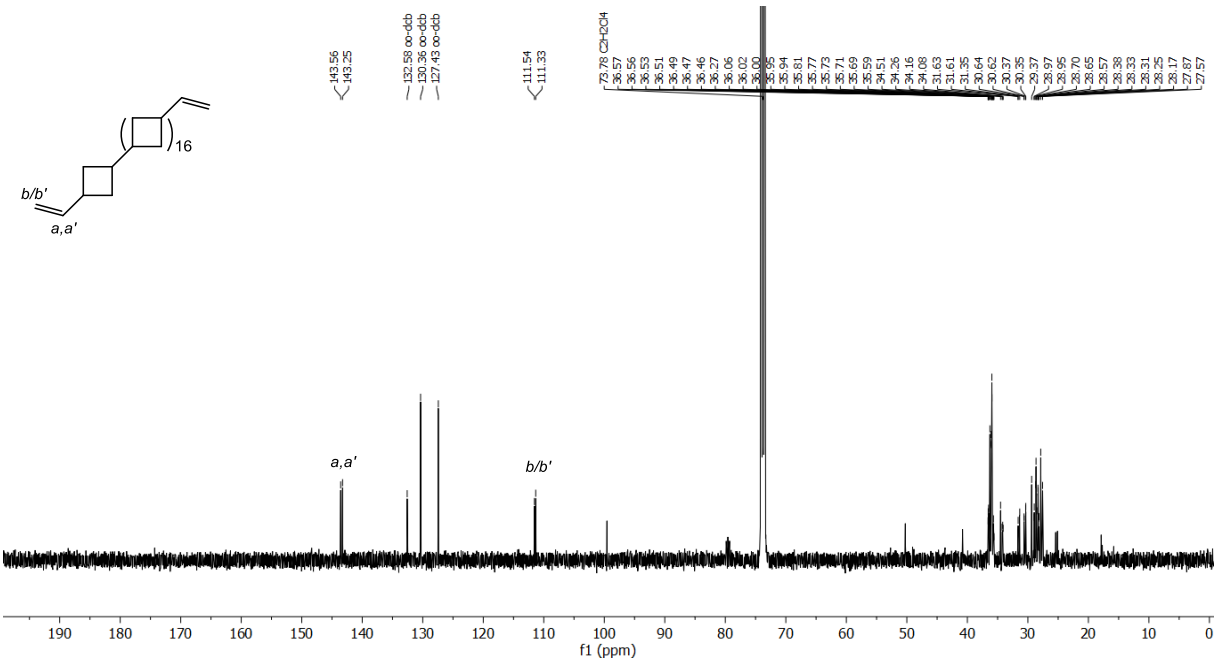

Figure 2B. ^{13}C{^{1}H} NMR (101 MHz, 1,1,2,2-tetrachloroethane-d_2, 120 ºC) spectrum of (1,n'-divinyl)oligocyclobutane (M_n ~ 973 g mol^{-1}, 17 cyclobutyls). Chain end assignments are given. Residual *o,o*-dichlorobenzene (o,o-dcb) from purification is present in the spectrum.

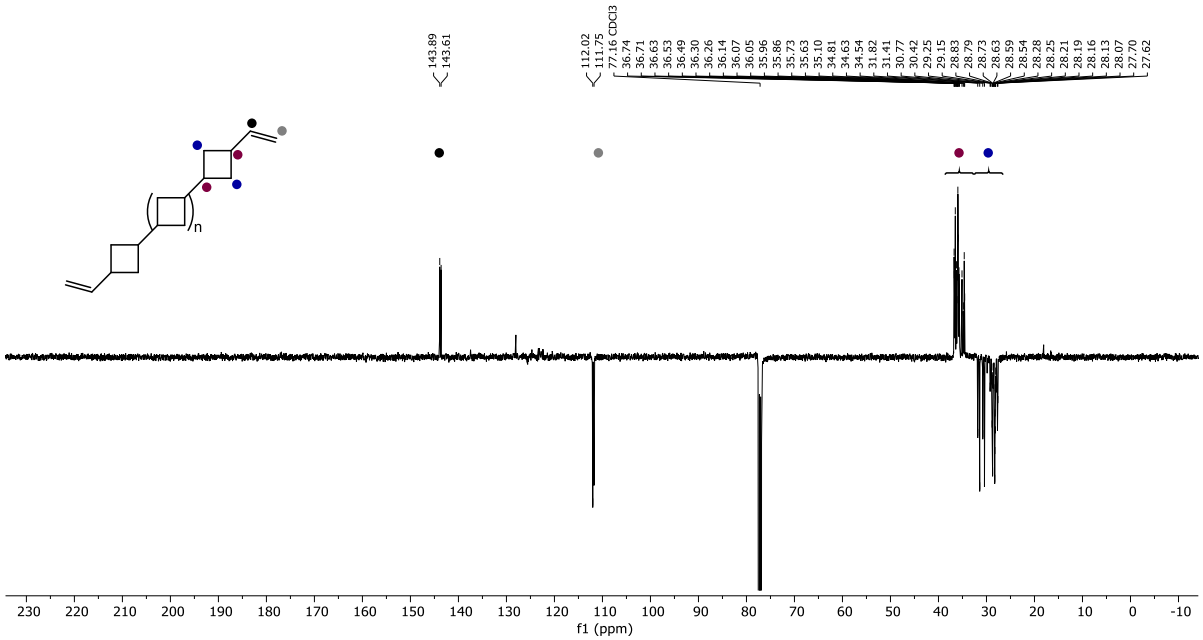

Figure 3A. $^{13}C\{^{1}H\}$ APT NMR (126 MHz, chloroform-*d*, 25 ºC) spectrum and partial assignment of (1,n'-divinyl)oligocyclobutane (M_n ~ 486 g mol^{-1}, 8 cyclobutyls).

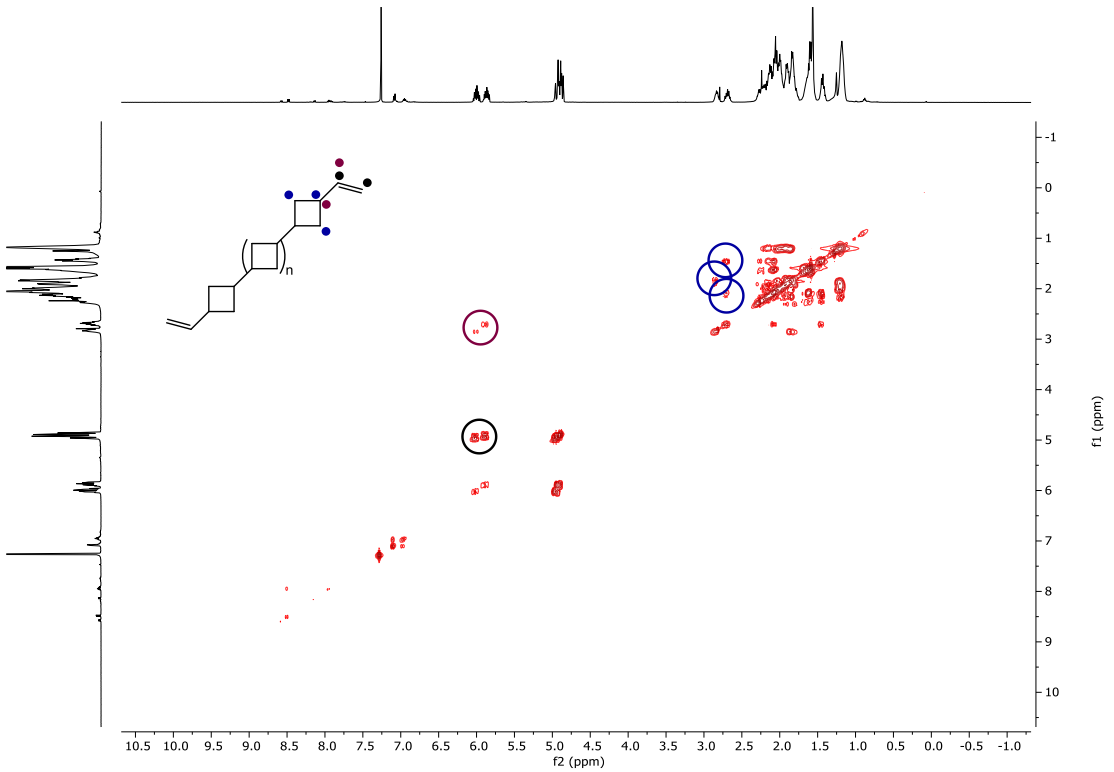

Figure 3B. ^{1}H-^{1}H COSY NMR (500 MHz, 500 MHz, chloroform-*d*, 25 °C) spectrum and partial assignment of (1,n'-divinyl)oligocyclobutane (M_n ~ 486 g mol^{-1}, 8 cyclobutyls).

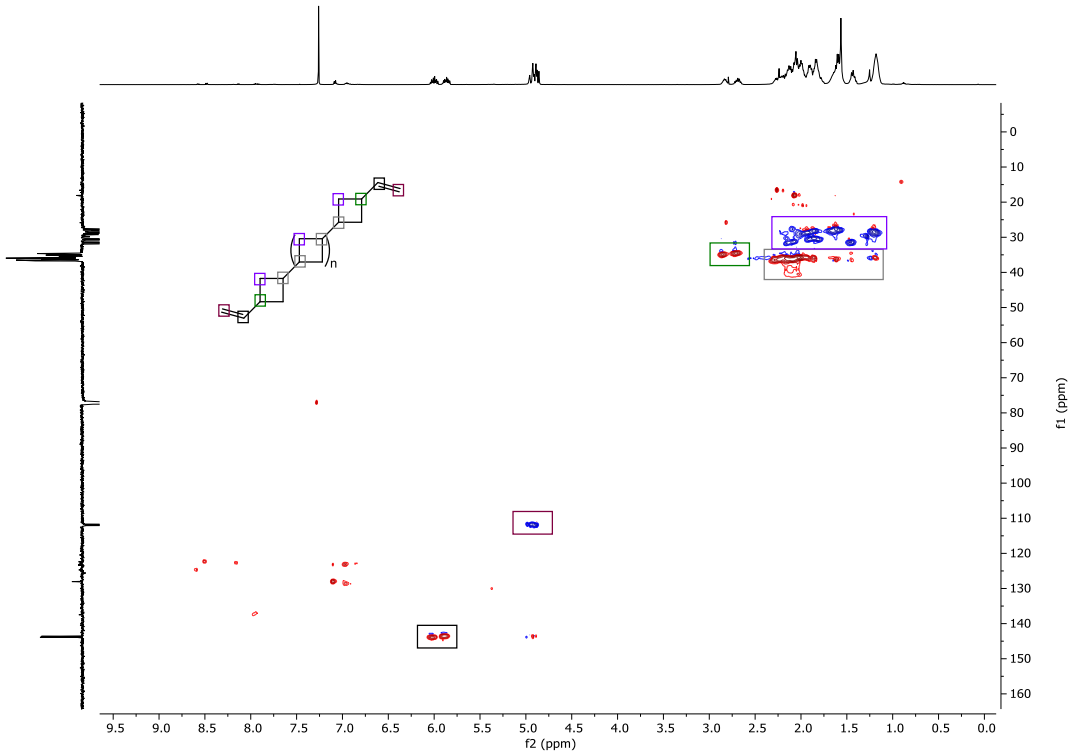

Figure 3C. ^{1}H-$^{13}C\{H\}$ HSQC NMR (500 MHz, 126 MHz, chloroform-*d*, 25 °C) spectrum and assignment of (1,n'-divinyl)oligocyclobutane (M_n ~ 486 g mol^{-1}, 8 cyclobutyls).

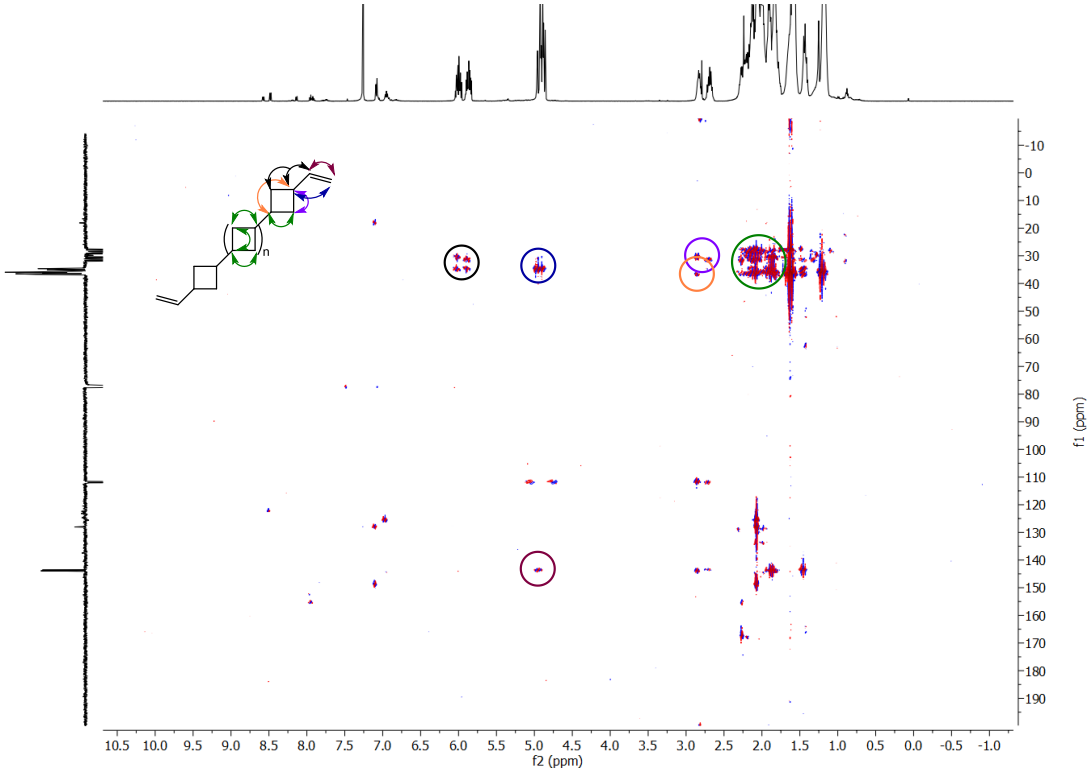

Figure 3D. ^{1}H-$^{13}C\{H\}$ HMBC NMR (500 MHz, 126 MHz, chloroform-*d*, 25 °C) spectrum and partial assignment of (1,n'-divinyl)oligocyclobutane (M_n ~ 486 g mol^{-1}, 8 cyclobutyls).

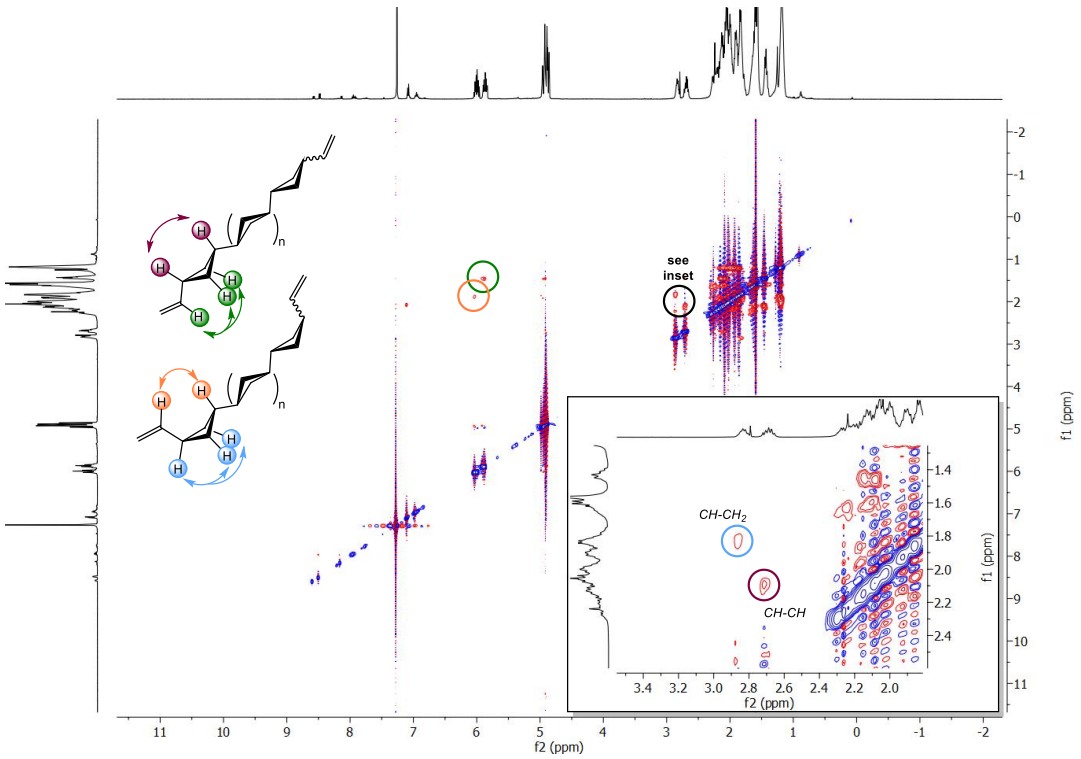

Figure 3E. ^{1}H-^{1}H NOESY NMR (500 MHz, chloroform-*d*, 25 °C) spectrum and depictions of observable correlations of two diastereomers of (1,n'-divinyl)oligocyclobutane (M_n ~ 486 g mol^{-1}, 8 cyclobutyls). Inset: expanded view of correlations corresponding to chain end 3° protons and cyclobutyl protons.

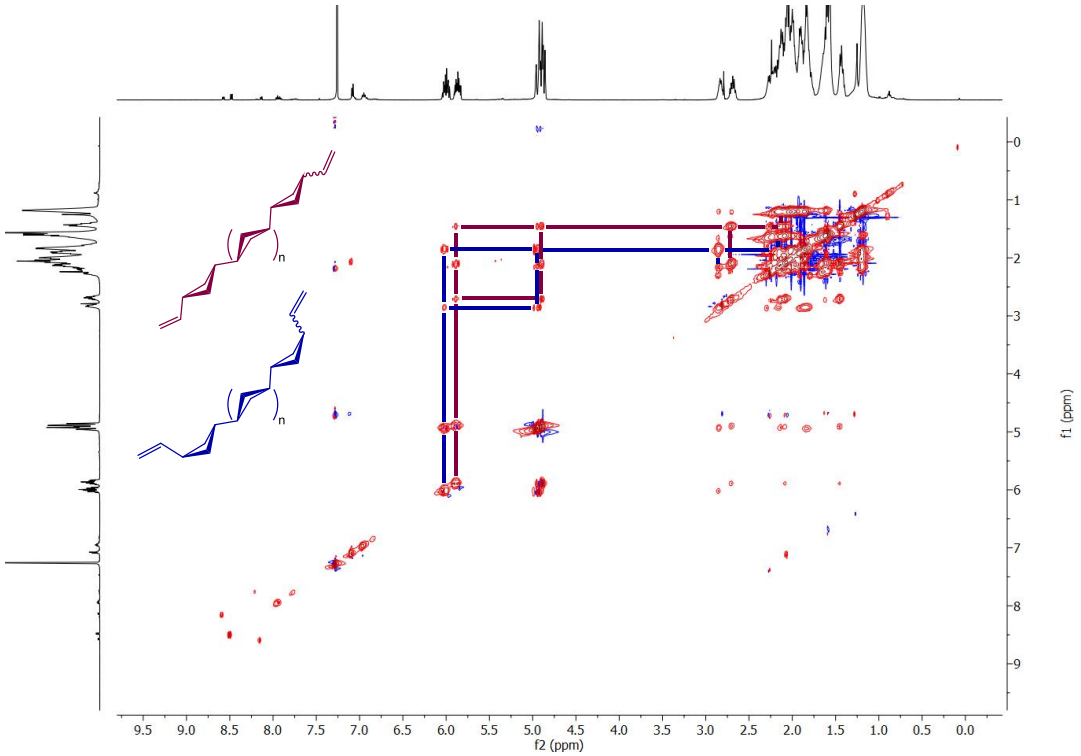

Figure 3F. ^{1}H-^{1}H TOCSY NMR (500 MHz, chloroform-*d*, 25 °C) spectrum and assignment of coupling networks of two observable diastereomers of (1,n'-divinyl)oligocyclobutane (M_n ~ 486 g mol^{-1}, 8 cyclobutyls).

Approximation of Molecular Weight by APCI-MS: Analysis of the molecular weight of both the ethyl acetate soluble and insoluble material was conducted using APCI-MS. 5 mg of ethyl acetate soluble (1,n'-divinyl)oligocyclobutane (M_n = 486 g mol^{-1}, 8 total cyclobutyls) was dissolved in approximately 1 mL of chloroform at room temperature and analyzed using an atmospheric sample analysis probe (ASAP). The resulting mass spectrum is given in Figure 4A. Similarly, a 10 mg sample of ethyl acetate insoluble (1,n'-divinyl)oligocyclobutane (Mn = 973 g mol^{-1}, 17 total cyclobutyls) was heated to 120 °C in 1 mL of *o,o*-dichlorobenzene (partial insolubility observed) and quickly injected with an ASAP. The resulting mass spectrum of the dissolved material is given in Figure 4B.

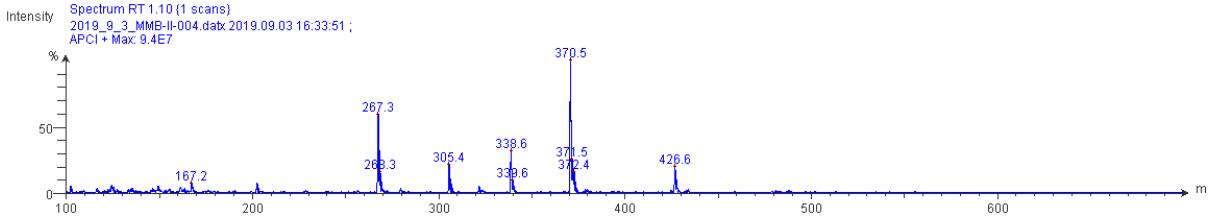

Figure 4A. APCI MS spectrum of ethyl acetate soluble (1,n'-divinyl)oligocyclobutane (M_n = 486 g mol^{-1}, 8 total cyclobutyls).

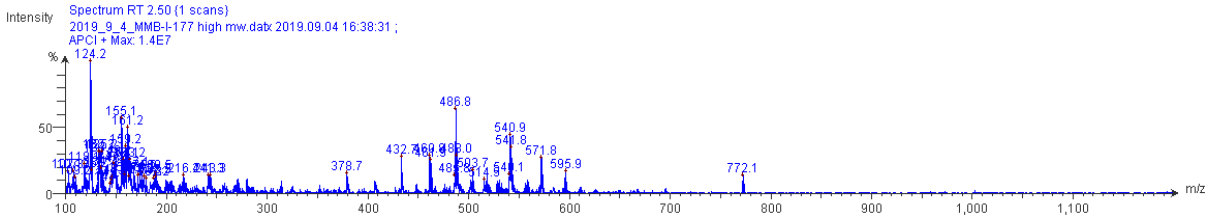

Figure 4B. APCI MS spectrum of solubilized ethyl acetate insoluble (1,n'-divinyl)oligocyclobutane (M_n = 973 g mol^{-1}, 17 total cyclobutyls). Partial insolubility of the solution was observed.

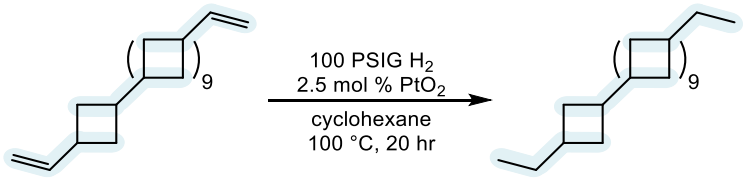

Spectroscopic data for (1,n'-diethyl)oligocyclobutane: ^{1}H NMR (400 MHz, 1,1,2,2-tetrachloroethane-d_2, 120 ºC): δ 2.29-1.27 (m, 57H), 0.87 (t, 6H, J coupling unresolved). The ^{1}H NMR is given in Figure 5A. ^{13}C{^{1}H} NMR (126 MHz, benzene-d_6, 25 ºC): δ 36.07, 35.89, 35.59, 32.75, 32.62, 30.89, 30.60, 29.75, 29.48, 29.25, 28.94, 28.58, 28.29, 27.95, 27.79, 27.49, 27.18, 26.37, 10.62, 10.36. The ^{13}C NMR is given in Figure 5B. The ATR spectrum is given in 5C.

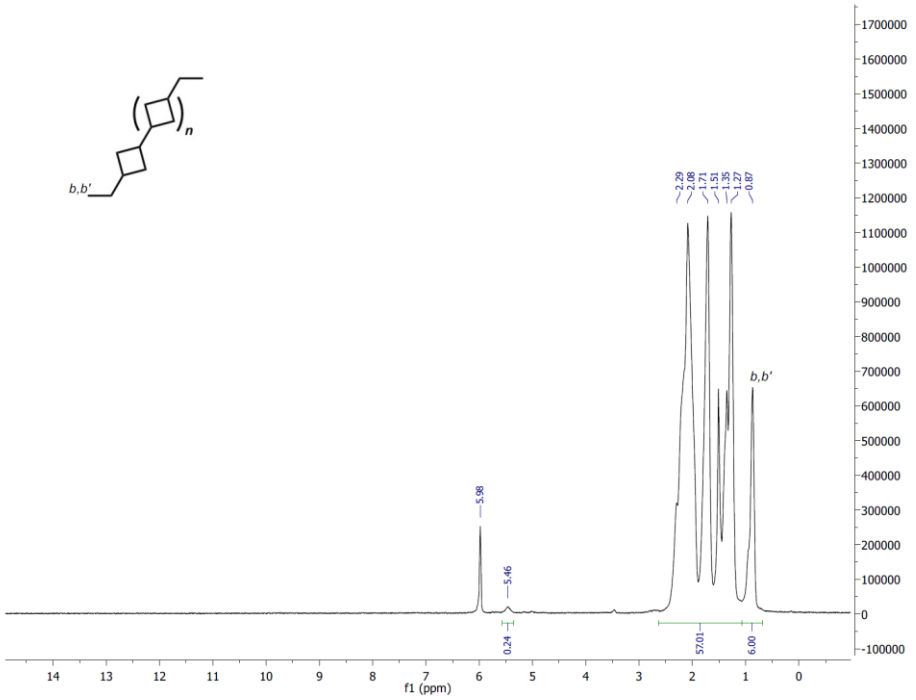

Figure 5A. ^{1}H NMR (400 MHz, 1,1,2,2-tetrachloroethane-d_2, 120 ºC) spectrum of (1,n'-diethyl)oligocyclobutane (M_n ~ 599 g mol^{-1}, 10 cyclobutyls). Chain end methyl assignments are given. A resonance corresponding to the vinyl CH_2 group in residual (1,n'-divinyl)oligocyclobutane is present at 5.46 ppm.

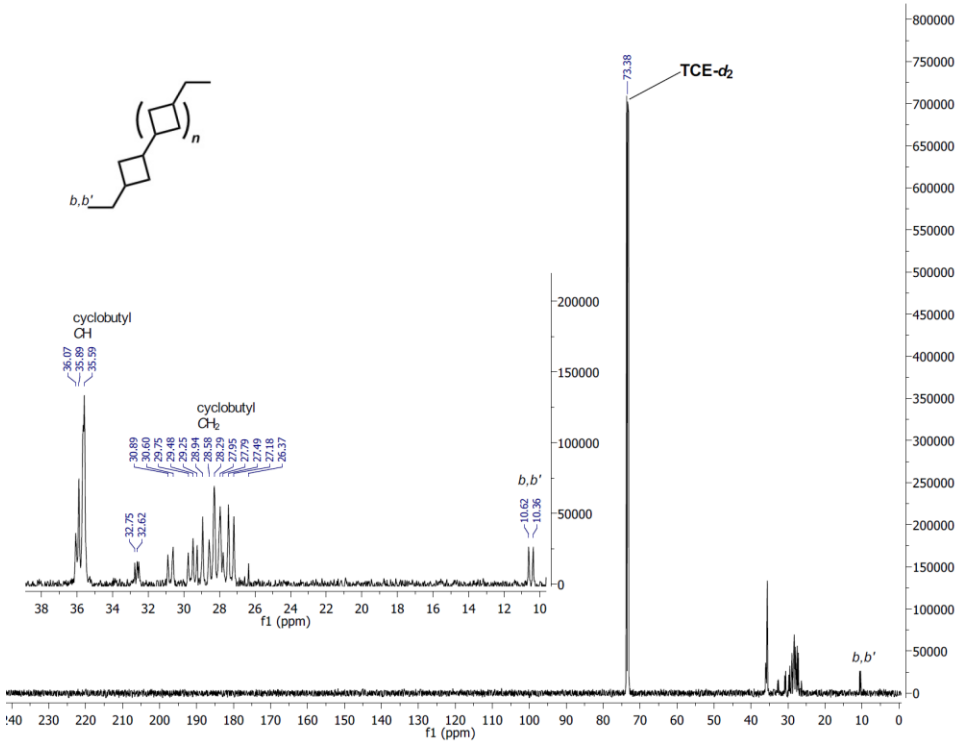

Figure 5B. ^{13}C NMR (101 MHz, 1,1,2,2-tetrachloroethane-d_2, 120 ºC) spectrum of (1,n'-diethyl)oligocyclobutane (M_n ~ 599 g mol^{-1}, 10 cyclobutyls). Chain end methyl assignments are given.

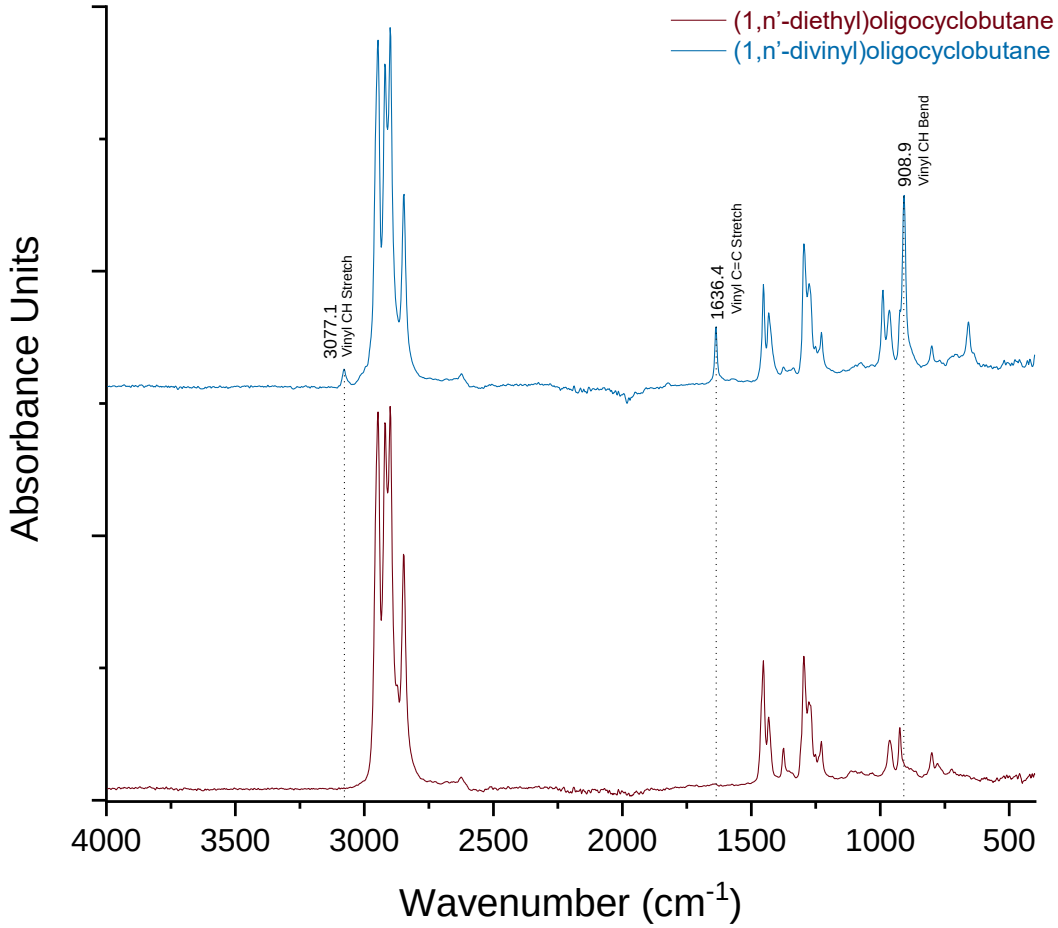

Figure 5C. Bruker Alpha ATR (single-bounce, diamond) of (1,n'-divinyl)oligocyclobutane (top) and its hydrogenated product, (1,n'-diethyl)oligocyclobutane. Peaks assignments corresponding to the vinyl functional group in (1,n'-divinyl)oligocyclobutane are shown.

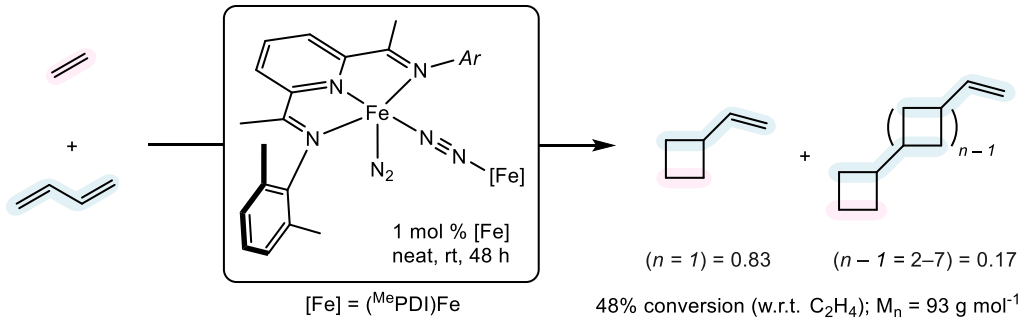

Identification of (n'-vinyl)oligocyclobutane: A 100 mL thick walled glass vessel containing a stir bar was charged with 47 mg (0.1 mmol) of $((^{Me}PDI)FeN_2)_2(\mu\text{-}N_2)$ in a nitrogen-filled glovebox. The flask was sealed, brought out of the glove box, and degassed on a high vacuum line. Butadiene (10 mmol) was added to the reaction vessel using a calibrated gas bulb. Without thawing the flask, ethylene (10 mmol) was added to the reaction vessel using a calibrated gas bulb. The flask was thawed and stirred at ambient temperature for 48 hours. Deposition of a liquid on the bottom of the flask was observed. In order to determine yield, the reaction vessel was vented, and 140 µL (1 mmol) of mesitylene internal standard was added to the mixture. An aliquot of the mixture was removed and analyzed by ^{1}H and ^{13}C NMR spectroscopy as well as GC. The yield was calculated relative to the mesitylene internal standard, and the number average molecular weight was determined by GC integrations corrected for number of carbons. The ^{1}H and ^{13}C NMR spectra are given in Figure 6A and 6B, respectively, and the GC is given in Figure 6C.

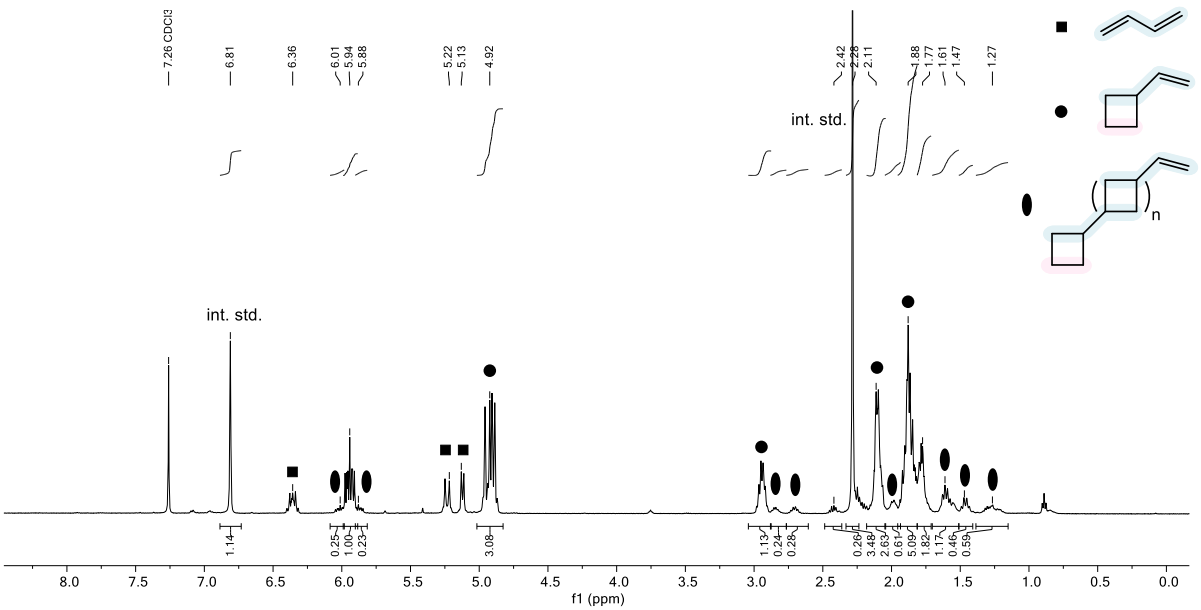

Figure 6A. ^{1}H NMR (500 MHz, chloroform-*d*, 25 ºC) spectrum of the [2+2] cycloaddition/oligomerization of ethylene and butadiene to produce (n-vinyl)oligocyclobutane (M_n ~ 93 g mol^{-1}).

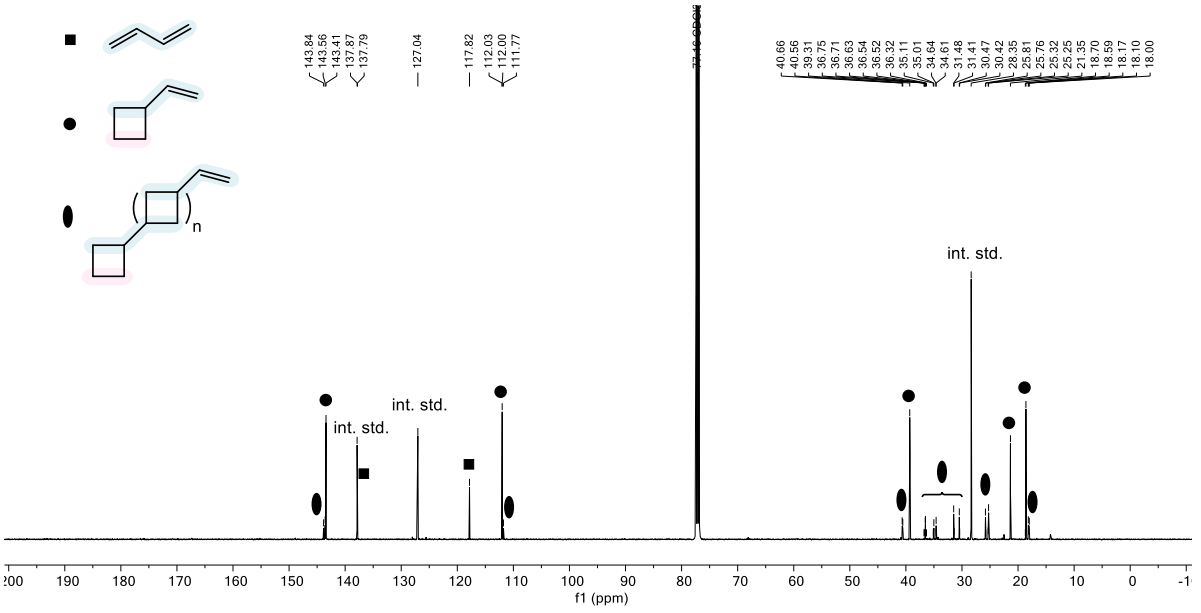

Figure 6B. ^{13}C NMR (126 MHz, chloroform-*d*, 25 ºC) spectrum of spectrum of the [2+2] cycloaddition/oligomerization of ethylene and butadiene to produce (n-vinyl)oligocyclobutane (M_n ~ 93 g mol^{-1}).

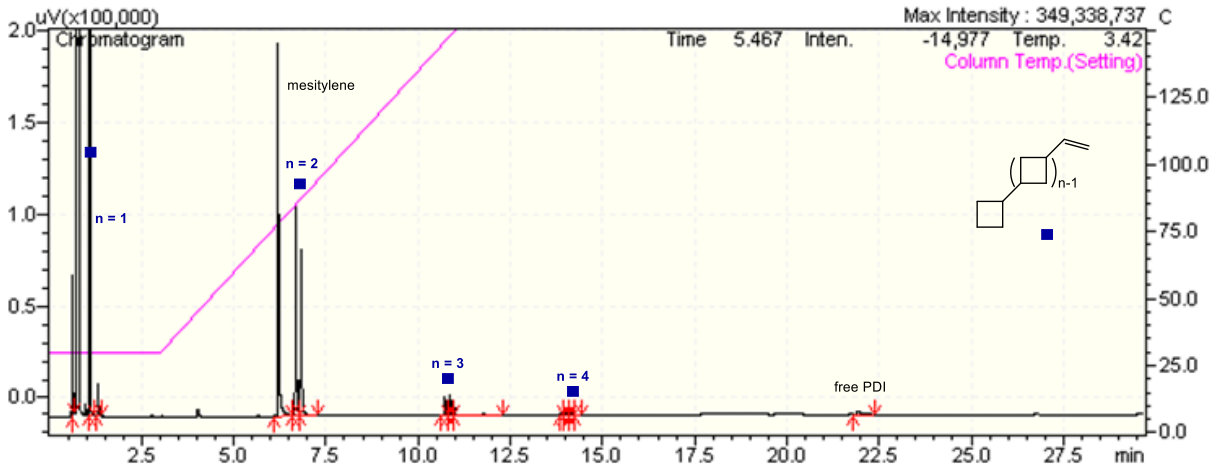

Retention Time	Area	Assignment	# carbons	Area/# carbons	Fraction	MW (g/mol)	Weighted MW (g/mol)
1.32	27115.9	n=1	6	4519.3	0.83	82.2	68.1845
6.196	490592	mesitylene	9	54510.2			
6.68	225561	n=2	10	22556.1	0.07756	136	10.56660301
6.826	200526.8	n=2	10	20052.7	0.06895	136	9.393853938
10.725	26153.9	n=3	14	1868.14	0.00642	190	1.222594438
10.868	38062.2	n=3	14	2718.73	0.00935	190	1.779261755
10.972	21139.7	n=3	14	1509.98	0.00519	190	0.988199834
13.873	2714	n=4	18	150.778	0.00052	244	0.126718733
14.004	5787.6	n=4	18	321.533	0.00111	244	0.270227465
14.155	3851.1	n=4	18	213.95	0.00074	244	0.179810801
14.265	873.7	n=4	18	48.5389	0.00017	244	0.04079372
21.942	10927.3	free PDI					
		oligomer		49440.4	1		92.75256369

Figure 6C. Gas chromatograph of the [2+2] cycloaddition/oligomerization of ethylene and butadiene to produce (n-vinyl)oligocyclobutane (M_n ~ 93 g mol^{-1}) and corrected GC integrations.

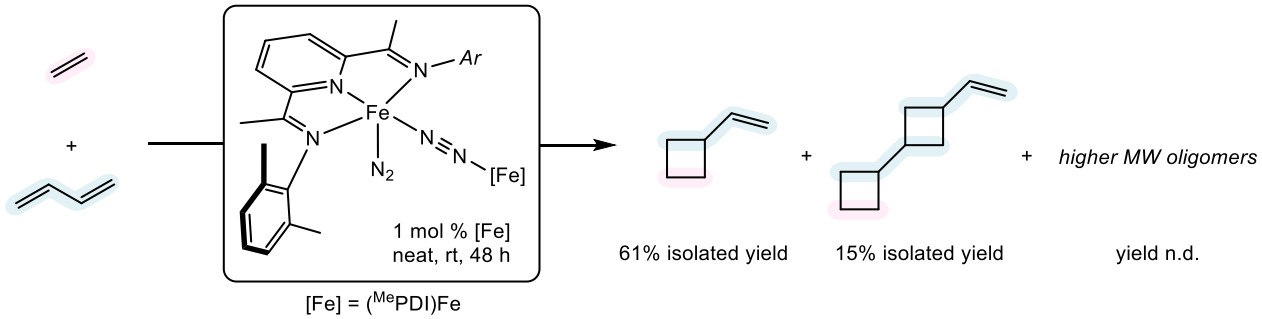

Spectroscopic data for 3-vinyl-1,1'-dicyclobutane: ^{1}H NMR (300 MHz, benzene-d_6, 25 ºC): δ 5.93 (m, 2H), 4.95 (m, 4H), 2.78 (app. p, J = 6.5 Hz, 1H), 2.65 (app. p, J = 5.6 Hz, 1H), 2.28 (app. sept., J = 7.4 Hz, 1H), 2.15 (m, 2H), 2.05 (m, 3H), 1.88 (m, 6H), 1.76 (m, 6H), 1.54 (m, 6H). Two diastereomers are observed. The ^{1}H NMR is given in Figure 7A. ^{13}C{^{1}H} NMR (126 MHz, benzene-d_6, 25 ºC): δ 143.65, 143.39, 112.31, 112.07, 40.91, 40.75, 36.80, 36.73, 35.31, 34.88, 31.65, 30.65, 26.02, 25.48, 18.43, 18.26. The ^{13}C NMR is given in Figure 7B.

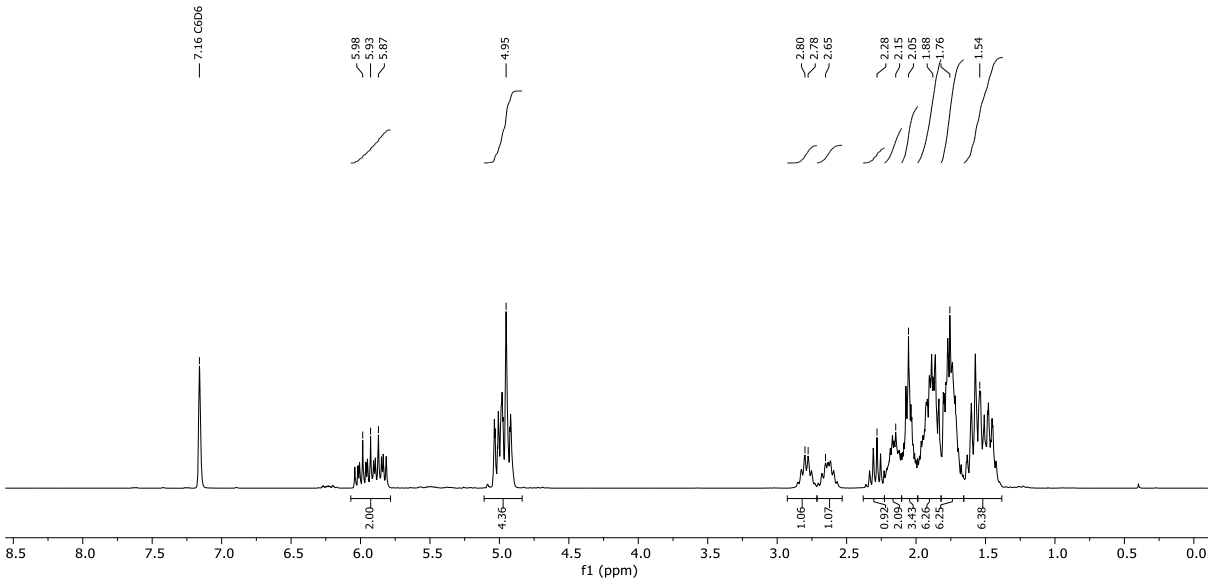

Figure 7A. ^{1}H NMR (300 MHz, benzene-*d*$_6$, 25 ºC) spectrum of 3-vinyl-1,1'-dicyclobutane. Two diastereomers are observed.

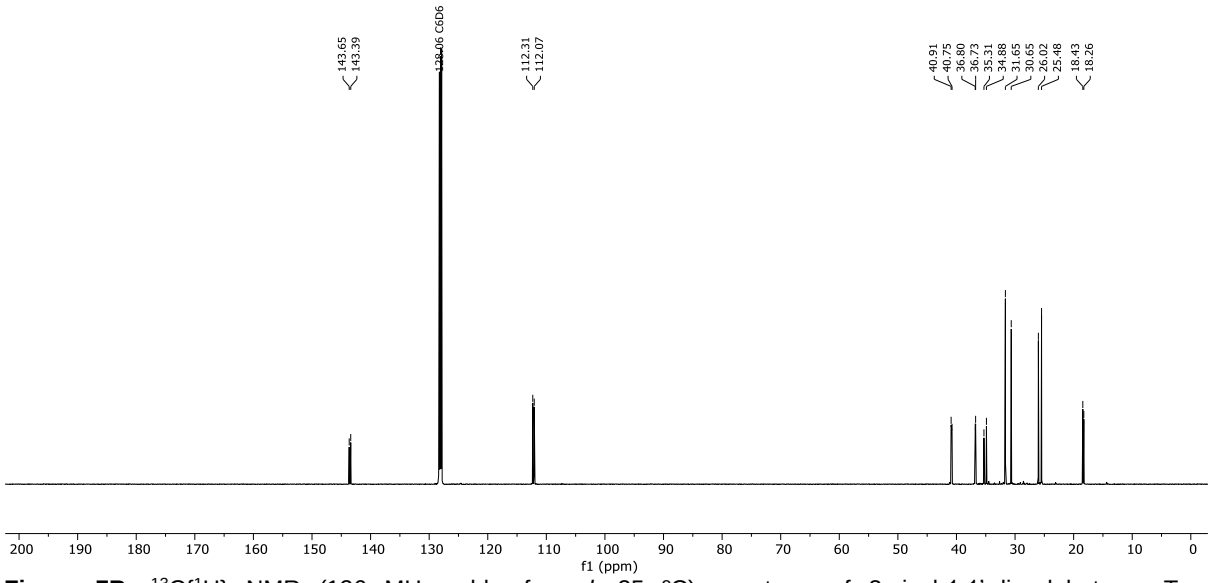

Figure 7B. ^{13}C{^{1}H} NMR (126 MHz, chloroform-*d*, 25 ºC) spectrum of 3-vinyl-1,1'-dicyclobutane. Two diastereomers are observed.

II. Additional NMR Spectroscopic Analysis

Additional information for ^{13}C spectroscopic assignments are provided for vinyl-dicyclobutane and (1,n'-divinyl)oligocyclobutane. DFT NMR simulations are also provided.

Additional spectroscopic data were collected on a (1,n'-divinyl)oligocyclobutane oligomer. Assignments were made based on high resolution NMR spectroscopic data and validated against NMR chemical shifts simulated by DFT. The sample was dissolved in deuterated 1,1,2,2-tetrachloroethane (tce-d_2) at a concentration of 67 mg mL^{-1} at 140°C. ^{1}H and ^{13}C NMR spectra were recorded at 120°C using a Bruker Avance IIIHD NMR spectrometer at 700/176 MHz respectively with a 10mm cryoprobe. Quantitative $^{13}C\{^{1}H\}$ NMR data were obtained using a 90° pulse, 60s delay, 512 transients, and inverse gated decoupling pulse sequence. A bi-waltz-65-256 decoupling scheme was used. To facilitate NMR spectroscopic assignments, DEPT-135, HMBQ experimental data were also collected. ^{1}H NMR data were referenced relative to protio residual of tce-d_2 (δ = 5.98 ppm). ^{13}C NMR data were reference relative to the carbon resonance of tce-d_2 (δ = 73.38 ppm).

Chemical Shift Assignments for 3-vinyl-1,1'-dicyclobutane:

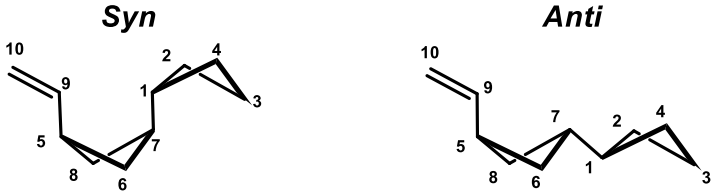

Table 1. ^{13}C NMR spectra assignments for 3-vinyl-1,1'-dicyclobutane.

Carbon Number & isomer	Functional group	chemical shift (δ ppm)
9 *anti*	vinyl CH	143.83
9 *syn*	vinyl CH	143.55
10 *syn*	vinyl CH2	112.03
10 *anti*	vinyl CH2	111.77
1 *syn*	CH ring	40.68
1 *anti*	CH ring	40.57
7 *anti*	CH ring	36.55
7 *syn*	CH ring	36.54
5 *anti*	CH ring	35.02
5 *syn*	CH ring	34.62
2,4 *syn*	CH2 ring	31.49
2,4 *anti*	CH2 ring	30.49
6,8 *anti*	CH2 ring	25.82
6,8 *syn*	CH2 ring	25.26
3 *syn*	CH2 ring end	18.17
3 *anti*	CH2 ring end	18.01

Stereochemical Assignments for (1,n'-divinyl)oligocyclobutane:

Diad and triad naming abbreviations for (1,n'-divinyl)oligocyclobutane oligomer:

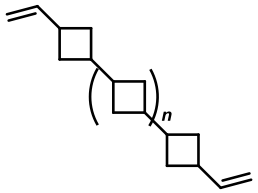

Each 1,3-substituted cyclobutane repeat unit may adopt either syn (s) or anti (a) configurations.

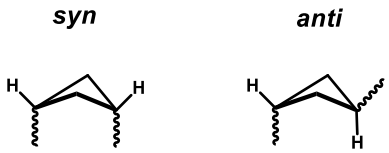

There are 4 possible diad combinations for the oligomer chain ends.

anti-anti (AA)

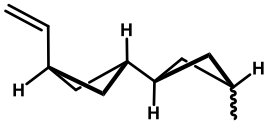

syn-syn (SS)

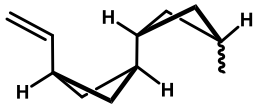

anti-syn (AS)

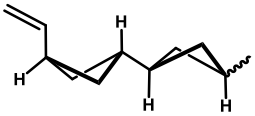

syn-anti (SA)

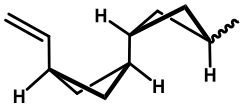

There are 6 unique triad sequences (SSA/ASS; and AAS/SAA are equivalent) for the oligomer backbone.

AAA

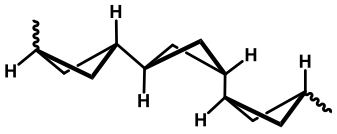

SSS

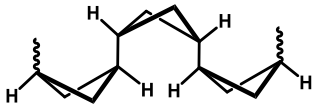

AAS or SAA

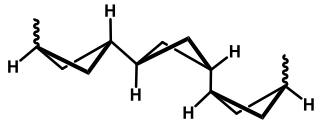

SSA or ASS

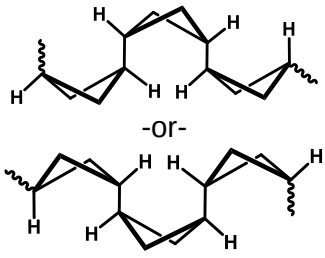

SAS

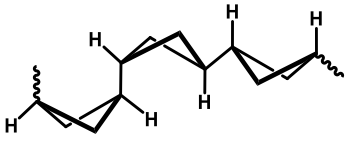

ASA

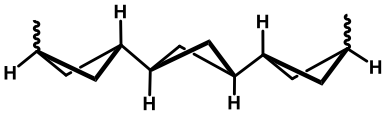

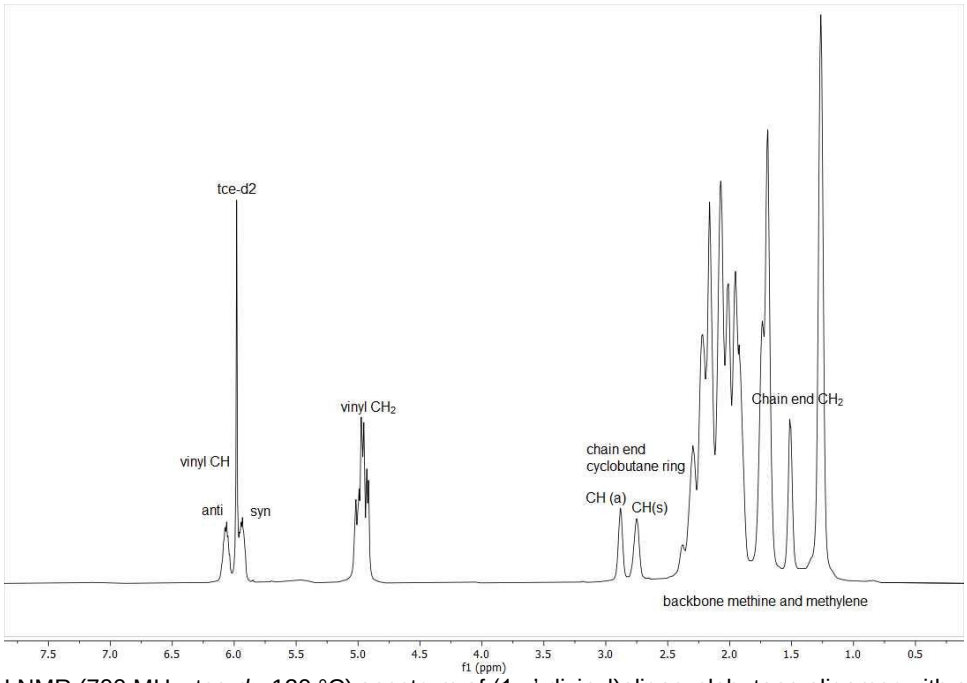

Figure 8A. ^{1}H NMR (700 MHz, tce-d_2, 120 °C) spectrum of (1,n'-divinyl)oligocyclobutane oligomer with assignments.

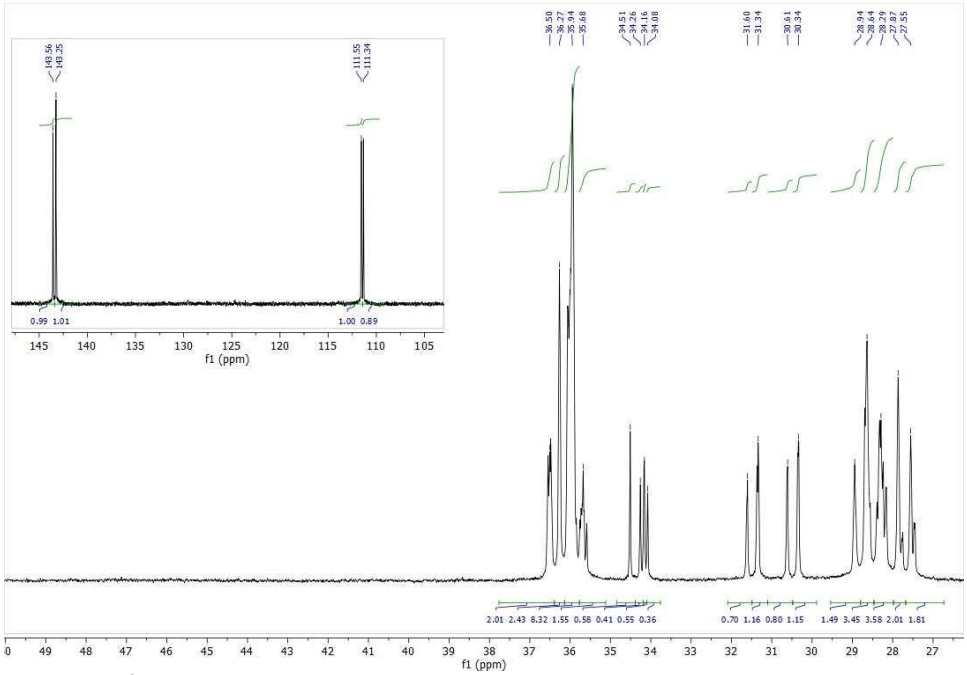

Figure 8B. Quantitative ^{13}C{^{1}H} NMR (176 MHz, tce-d_2, 120 °C) spectrum of (1,n'-divinyl)oligocyclobutane oligomer. Inset: expanded view of vinyl region.

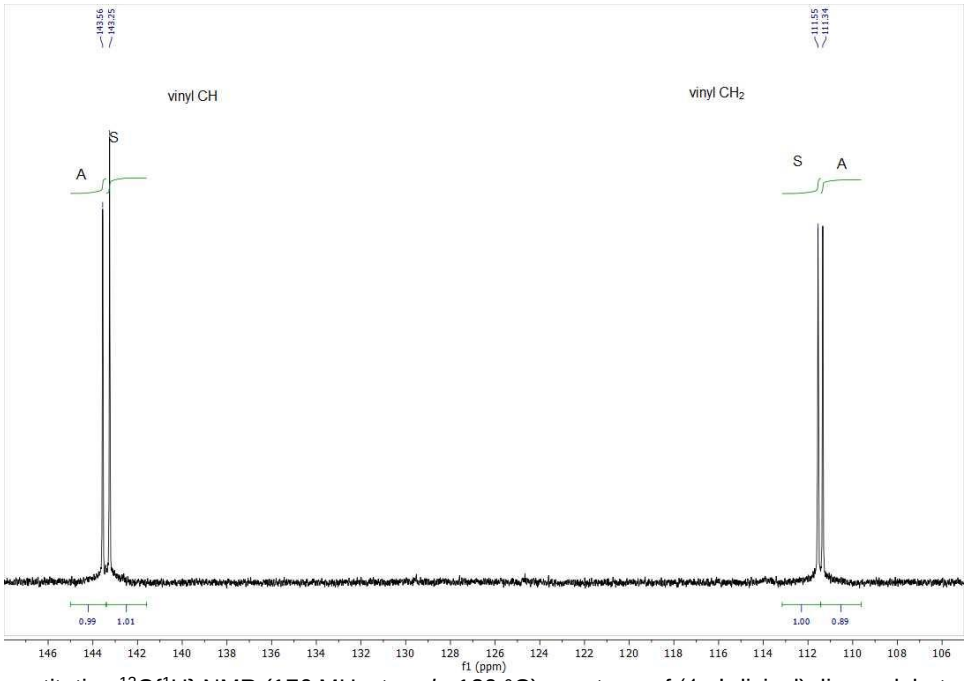

Figure 8C. Quantitative $^{13}C\{^{1}H\}$ NMR (176 MHz, tce-d_2, 120 °C) spectrum of (1,n'-divinyl)oligocyclobutane oligomer. Enlarged view of chain end vinyl region with diad assigments.

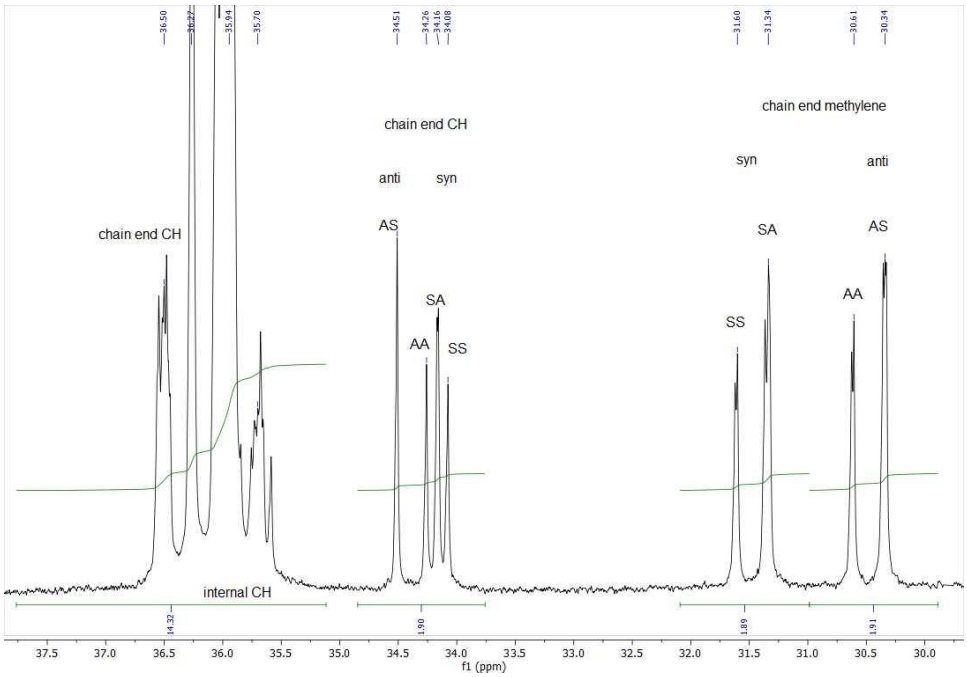

Figure 8D. Quantitative $^{13}C\{^{1}H\}$ NMR (176 MHz, tce-d_2, 120 °C) spectrum of (1,n'-divinyl)oligocyclobutane oligomer. Enlarged view C-H resonances. Diad assignments are provided for chain ends.

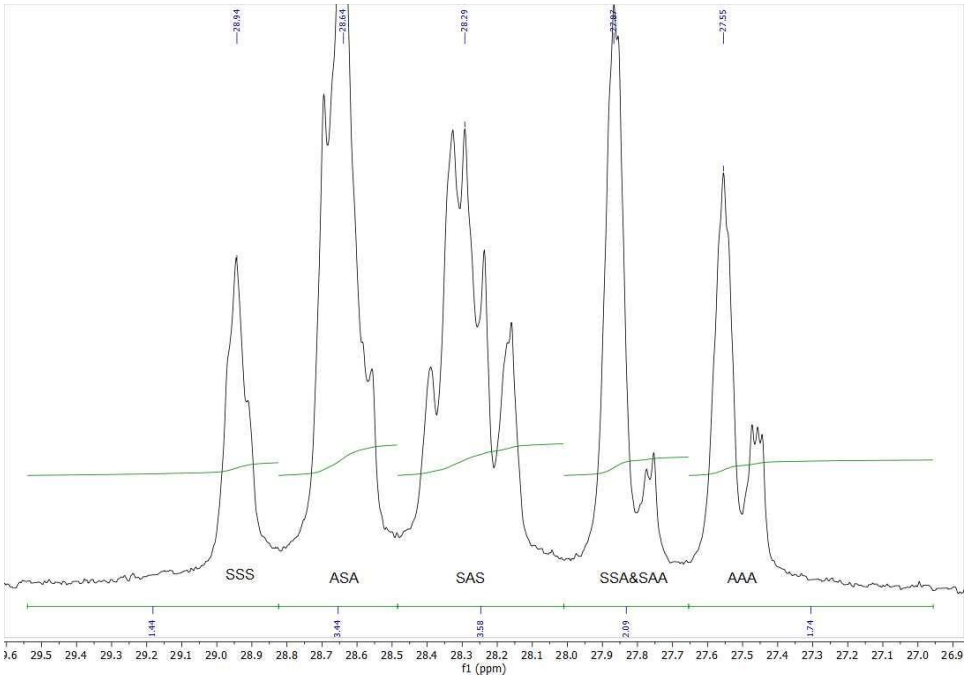

Fig. 8E. Quantitative $^{13}C\{^{1}H\}$ NMR (176 MHz, tce-d_2, 120 °C) spectrum of (1,n'-divinyl)oligocyclobutane oligomer. Enlarged view backbone CH_2 resonances. Triad assignments are provided.

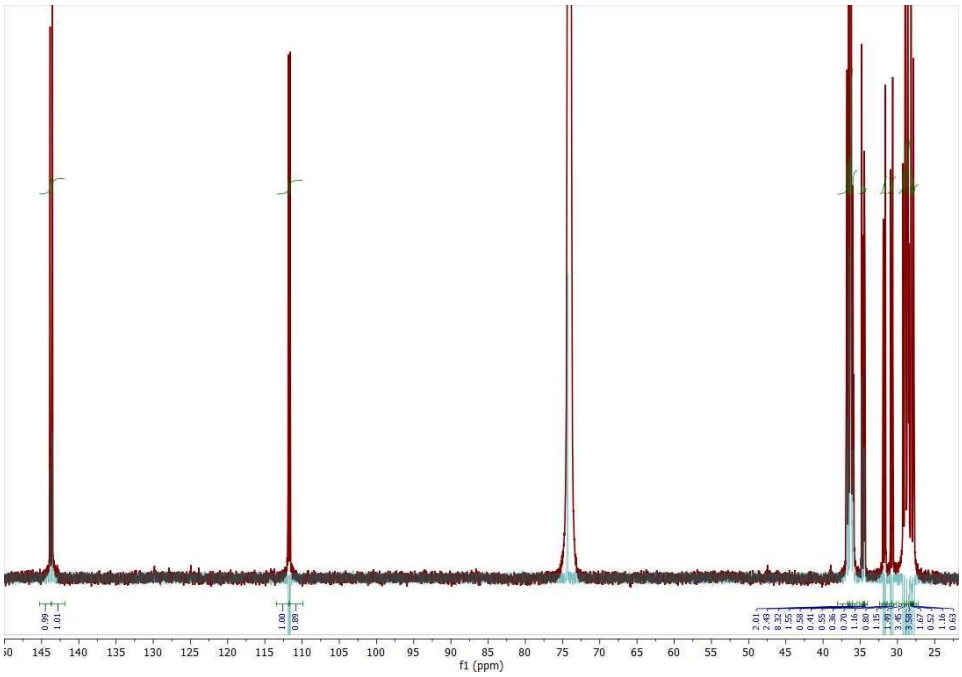

Fig. 8F. DEPT-135 edited NMR spectrum (blue) overlaid with $^{13}C\{^{1}H\}$ NMR (176 MHz, tce-d_2, 120 °C) spectrum (red) of (1,n'-divinyl)oligocyclobutane oligomer.

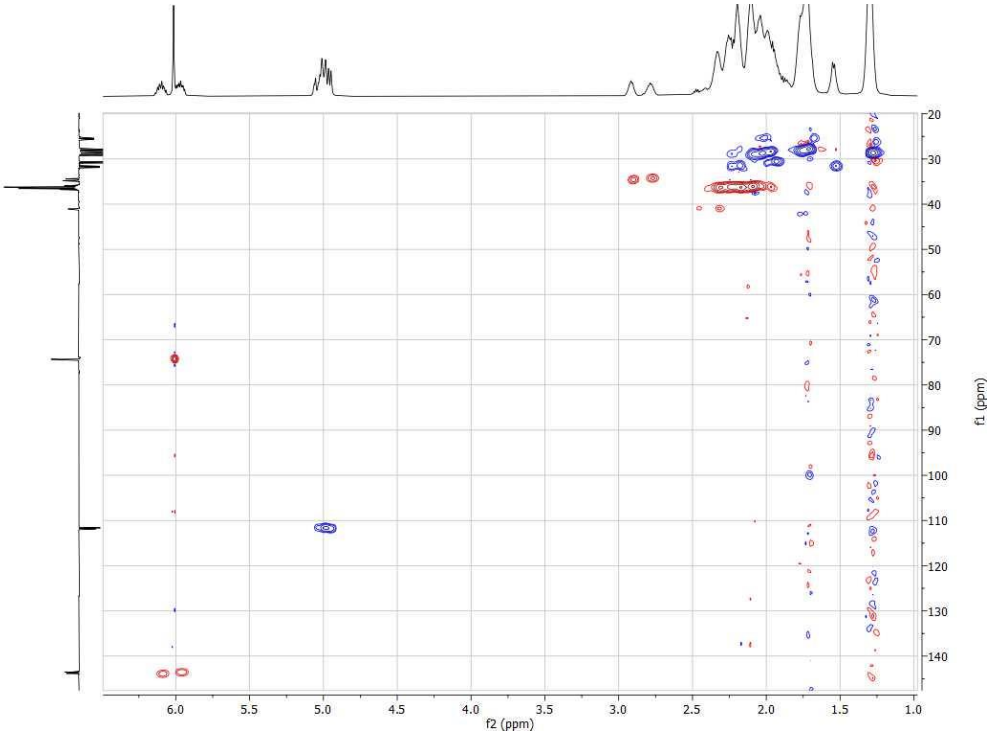

Figure 8G. DEPT-135-edited HSQC (tce-d_2, 120 °C) spectrum of (1,n'-divinyl)oligocyclobutane oligomer.

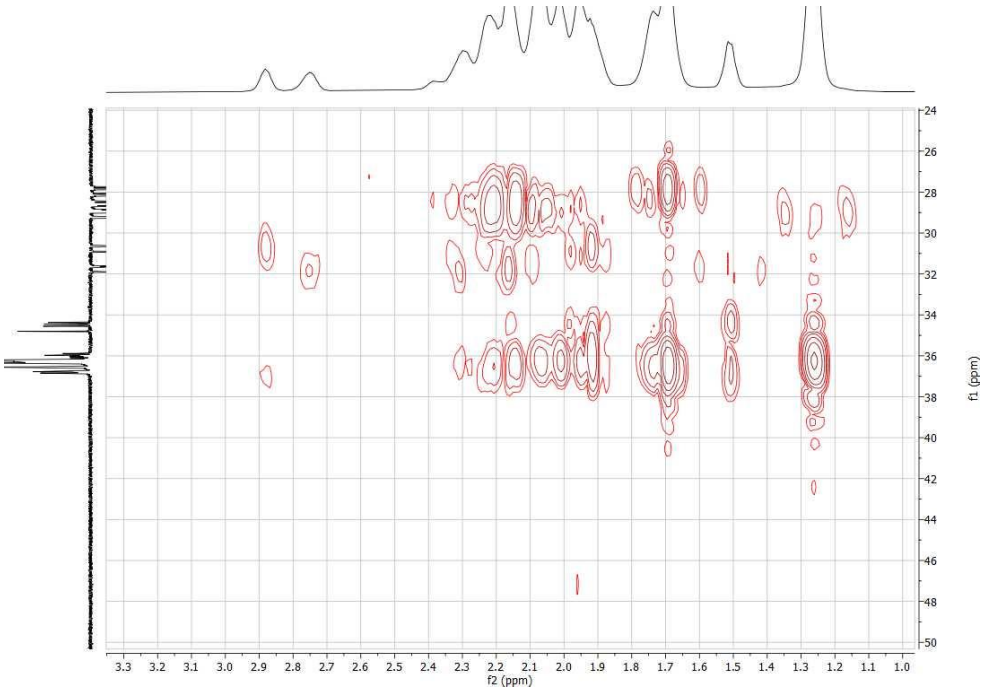

Figure 8H. HMBC (tce-d_2, 120 °C) spectrum of (1,n'-divinyl)oligocyclobutane oligomer.

Table 2. Sequence distribution summary for of (1,n'-divinyl)oligocyclobutane oligomer from the analysis of ^{1}H and $^{13}C\{^{1}H\}$ NMR spectroscopic data.

Sequence distribution information from quantitative $^{13}C(^{1}H)$ NMR (tce-d_2, 120 °C)			
vinyl CH		**vinyl CH_2**	
anti	49.5%	*anti*	47.1%
syn	50.5%	*syn*	52.9%
diad (using chain end CH)			
aa	30.5%	sa	28.9%
as	21.6%	ss	18.9%
triad (using oligomer chain CH_2)			
sss	12.1%	ssa & saa	16.4%
asa	27.9%	aaa	14.9%
sas	28.7%		
Sequence distribution information from ^{1}H NMR (tce-d_2, 120 °C)			
anti	47.4%	*syn*	52.6%

DFT NMR Simulations: To validate the proposed poly(cyclobutane) structure and facilitate spectroscopic assignments, ^{13}C NMR chemical shifts were simulated by DFT for isomers of both 3-vinyl-1,1'-dicyclobutane and a 3,3''-divinyl-1,1':3',1''-tercyclobutane trimer.

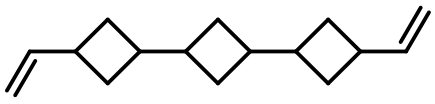

DFT-predicted ^{13}C NMR shifts were calculated using Jaguar v10.6 release 12 with geometries optimized using the B3LYP-D3 functional and the 6-311G** basis set, where D3 is the two-body Grimme dispersion correction.[1-8] Additional polarization (*) functions follow standard conventions. All shifts are given relative to DFT-predicted TMS (184.39 ppm). DFT-predicted shifts for the *syn* and *anti* vinyl dimer were regressed linearly against the experimental NMR assignments (slope =

0.982, intercept = -5.206, standard error = 1.679, R^2 = 0.998) and these are the values reported in Table 3. DFT-predicted shifts for the 3,3''-divinyl-1,1':3',1''-tercyclobutane trimers models utilized same linear correction shown above. DFT coordinate files can be found as supplementary mae files.

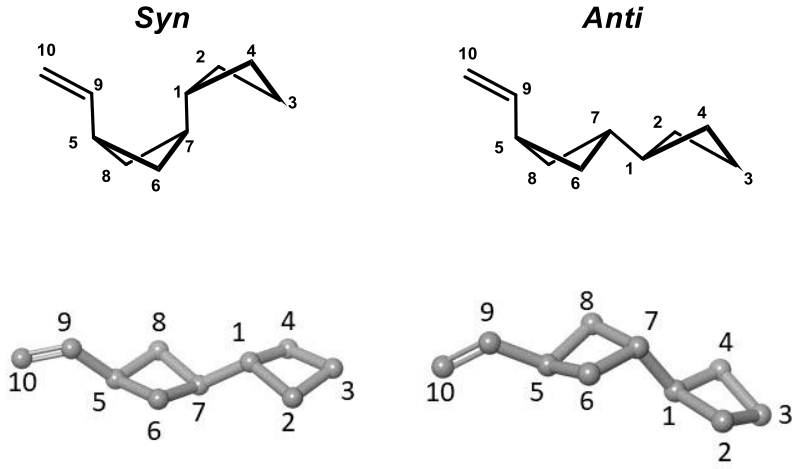

Figure 9. DFT simulated *syn* and *anti* 3-vinyl-1,1'-dicyclobutane groups.

Table 3. DFT simulated chemical shifts for 3-vinyl-1,1'-dicyclobutane and experimentally observed values (tce-d_2).

	DFT Simulated *syn* isomer (ppm)	*syn* isomer Experimental (ppm)	DFT Simulated *anti* isomer (ppm)	*anti* isomer experimental (ppm)
C1	42.94	40.68	39.63	40.57
C2	25.34	25.82	25.23	25.26
C3	15.78	18.17	15.16	18.01
C4	25.34	25.82	25.21	25.26
C5	36.69	34.62	37.16	35.02
C6	32.40	31.49	29.70	30.49
C7	38.73	36.54	37.77	36.54
C8	32.35	31.49	29.66	30.49
C9	144.54	143.55	144.60	143.83
C10	109.72	112.03	109.48	111.77

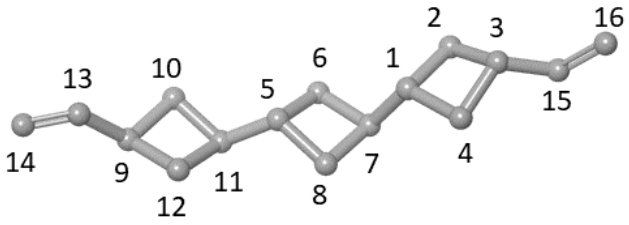

Figure 10. Simulated 3,3''-divinyl-1,1':3',1''-tercyclobutane oligomer (sas) showing carbon numbering scheme.

Table 4. Simulated chemical shifts for 3,3''-divinyl-1,1':3',1''-tercyclobutane triad sequences. Chemical shifts are reported in ppm.

	Functional Group	aaa	asa	saa	sas	ssa	sss
C1	internal CH	35.45	38.88	35.66	35.77	39.15	39.36
C2	internal CH_2	30.71	30.92	32.39	32.53	32.45	32.45
C3	chain end CH	35.22	36.02	36.14	36.15	36.65	36.76
C4	internal CH_2	30.89	30.89	32.36	32.52	32.48	32.44
C5	internal CH	38.29	38.38	38.92	38.61	37.90	37.69
C6	internal CH_2	27.35	30.09	27.52	27.51	30.07	30.13
C7	internal CH	37.30	38.38	36.93	36.99	37.78	37.63
C8	internal CH_2	27.45	30.06	27.51	27.48	30.01	30.10
C9	chain end CH	35.74	36.04	35.95	36.50	36.15	36.51
C10	internal CH_2	30.65	30.90	30.77	32.41	30.75	32.50
C11	internal CH	39.19	38.82	38.71	38.87	39.22	39.37
C12	internal CH_2	30.74	30.87	30.76	32.44	30.83	32.41
C13	vinyl CH	144.04	144.23	143.92	144.88	143.72	144.96
C14	vinyl CH_2	109.02	108.93	108.94	109.82	108.95	109.78
C15	vinyl CH	144.10	144.16	144.59	144.96	144.63	144.58
C16	vinyl CH_2	108.87	108.94	109.84	109.73	109.76	109.82

III. Oligomerization Conditions Screening

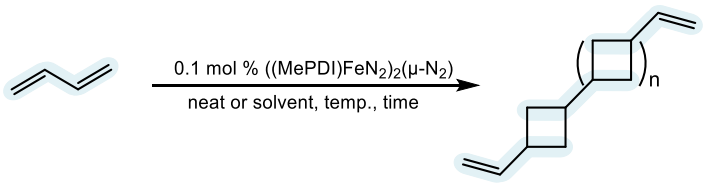

Butadiene Purification: Butadiene was liquefied and cooled to -30 °C, after which it was filtered through a medium porosity fritted funnel containing basic alumina into a chilled round-bottom flask. The butadiene was then vacuum transferred into a receiving flask which was stored cold in the absence of light.

Oligomerization Procedure for Neat Reaction Screening (Entries 1-3): A thick-walled round-bottom flask was fitted with PTFE-coated magnetic stir bar and charged with 6.5 g butadiene ± 0.5 g. Catalyst (0.112 g, 0.1 mol %) was then added as a microcrystalline powder. The flask was sealed and brought to 50 °C where it was allowed to react for 40 h. After 24 h, colorless precipitate was observable. For entries 2 and 3, the reaction mixture was predominantly solid with small quantities of unreacted butadiene vapor. The flask was then vented and the remainder of the work-up conducted in air. The reaction contents were combined with ethyl acetate (50 mL) and transferred to a beaker (50 mL) were they were stirred vigorously for 1 h to de-ash the solid polymer. The resulting suspension was filtered through a medium porosity fritted funnel. This afforded a pale, tan-colored precipitate and a pale yellow filtrate. The insoluble material was collected and dried under reduced pressure. Polymer yield was recorded and the M_n measured by ^{1}H NMR spectroscopy (tce-d_2, 120°C). Percent yield is calculated based on butadiene.

Oligomerization Procedure for Reaction Screening with Solvent (Entry 4): A thick-walled round-bottom flask was fitted with PTFE-coated magnetic stir bar and charged with 3.0 g butadiene ± 0.5 g. A cyclohexane solution (30 mL) of ($(^{Me}PDI)FeN_2)_2(\mu\text{-}N_2$) (0.052 g, 0.1 mol %)

was then added. The flask was then sealed and brought to 50 °C where it was allowed to react for 40 h. After 24 h, no p was observable. After 40 h, the reaction mixture was cooled to room temperature and vented. The remainder of the work-up was conducted in air. No polymer precipitate was visible. The liquid volume (30 mL) and mass (21.756 g) were recorded. To this mixture *n*-nonane (1 g) was added as an internal standard and the mixture analyzed by GC-MS, indicating no trace of product formation (Figure 11).

Table 5. Oligomerization condition screening results.

Entry	Solvent	Mass Butadiene (g)	Catalyst Loading (mol %)	Temp (°C)	Time (h)	EtOAc insol. yield (g)	Yield (%)	M_n (g·mol^{-1}); [# cyclobutyls]
1	Neat	6.5	0.1	30	50	0.03	4.6	485 [7.5]
2	Neat	6.5	0.1	50	40	3.08	47	581 [9.8]
3	Neat	6.5	0.1	70	2	2.28	35	633 [10.7]
4	Cyclohexane	3.0	0.1	50	40	–	–	–

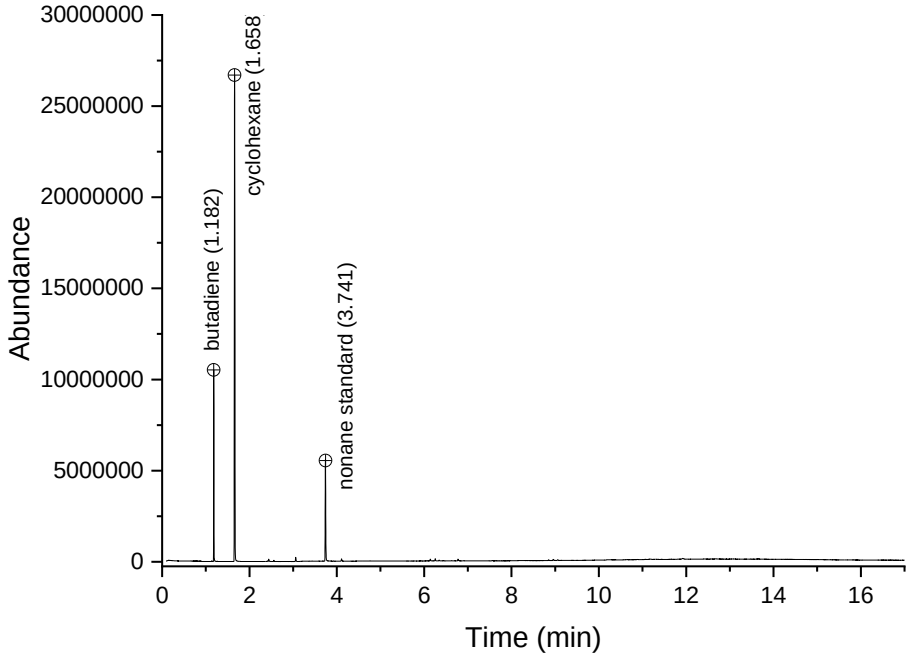

Figure 11. GC-MS chromatogram trace for the liquid product mixture obtained from Entry 4. No appreciable quantities of low-molecular oligomers were observed. GC-MS method calibrated to detect up to C_{24}.

IV. Precatalyst Screening

General Procedure for Precatalyst Screening: Reaction mixtures were prepared as detailed in **the Methods section, Preparation of (1,n')-divinyl-oligocyclobutane**. After 72 hours, the reactions were quenched by vacuum transferring the volatiles into a flask containing 800 – 1000 µL of chloroform-*d* for analysis by ^{1}H NMR. The nonvolatiles (if applicable) were extracted with approximately 10 mL of ethyl acetate. The ethyl acetate soluble fractions (if applicable) were decanted away from the insoluble material (if formed) and passed through a pipet plug containing ~ 5 cm of silica, eluting with additional ethyl acetate. Both fractions were evaporated to dryness. Both the ethyl acetate soluble and insoluble materials were analyzed by ^{1}H NMR as detailed in Supplementary Information, **Section I**, and M_n and diastereomeric ratio (d.r.) for the two observed diastereomers were determined from relative ^{1}H NMR integrations. The tabulated data are given in Table 6.

Table 6. Scope of precatalysts examined for the [2+2] cycloaddition/oligomerization of butadiene.

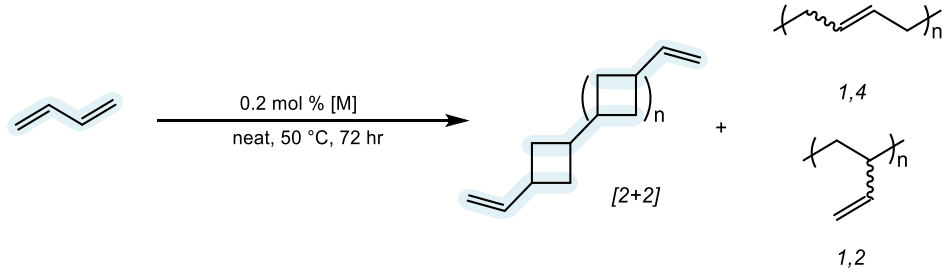

Entry	[M]	avg. n	M_n	d.r.	Other products detected
1	[(^{Me}PDI)Fe(N_2)]$_2$(μ-N_2)	16	973	1:1	-
2	[($^{Me(Et)}$PDI)Fe(N_2)]$_2$(μ-N_2)	12	757	1:1	-
3	(^{iPr}PDI)Fe(N_2)$_2$	4	324	1:1	-
4	($^{iPr(TB)}$PDI)Fe(N_2)$_2$	n.d	n.d	n.d	-
5	(^{iPr}PDAI)Fe(C_4H_6)	n.d	n.d	n.d	-
6	(^{Me}PDI)Fe(C_4H_6)	12	757	1:1	-
7	(^{Me}PDI)FeCl_2 + Mg(C_4H_6)·2THF[a]	14	865	1:1	1,4
8	(^{Mes}CNC)Fe(N_2)$_2$	n.d.	n.d.	n.d.	-
9	[(dppf)Co(toluene)]BAr$^F{}_4$	n.d.	n.d.	n.d.	1,2

n.d. = none detected.
[a.] 1 mol % [Fe], 1.1 mol % Mg(C_4H_6)·2THF

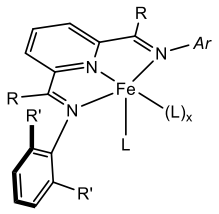

R = Me, R' = Me, L = N_2, x = 0.5: [(^{Me}PDI)Fe(N_2)]$_2$(μ-N_2)
R = Et, R' = Me, L = N_2, x = 0.5: [($^{Me(Et)}$PDI)Fe(N_2)]$_2$(μ-N_2)
R = Me, R' = ^{i}Pr, L = N_2, x = 1: (^{iPr}PDI)Fe(N_2)$_2$
R = Me, R' = Me, L = Cl, x = 1: (^{Me}PDI)FeCl_2

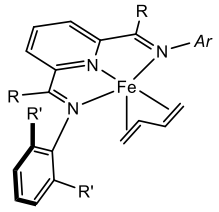

R = Me, R' = Me: (^{Me}PDI)Fe(C_4H_6)
R = H, R' = ^{i}Pr: (^{iPr}PDAI)Fe(C_4H_6)

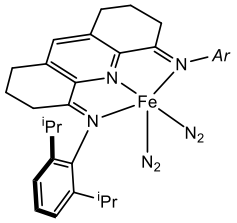

($^{iPr(TB)}$PDI)Fe(N_2)$_2$

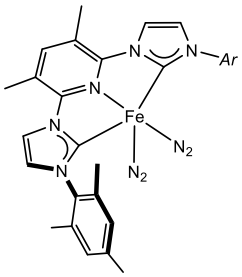

(^{Mes}CNC)Fe(N_2)$_2$

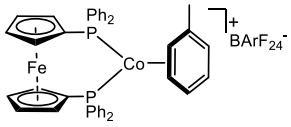

[(dppf)Co(toluene)]BAr$^F{}_4$

V. Wide-Angle X-ray Scattering and Polymorph MD Simulation

Data Collection and Reduction: A powder sample of (1,n'-divinyl)oligocyclobutane (M_n ~ 973 g mol^{-1}, 17 total cyclobutyls) was held between two sheets of ~ 6 μm thick mica in a small cell attached to a Linkam HSFX350 heating stage in vacuum. The 2D scattering patterns were first masked of any single-crystal diffraction peaks appearing from the mica windows. The sample was cooled from 170°C at 10°C/min and allowed to equilibrate for 5 minutes at each temperature before the scattering pattern was collected (Figure 12A and 12B). The images were then integrated and reduced to 1D patterns which were fit in order to extract the rotator, crystalline, and amorphous contributions.

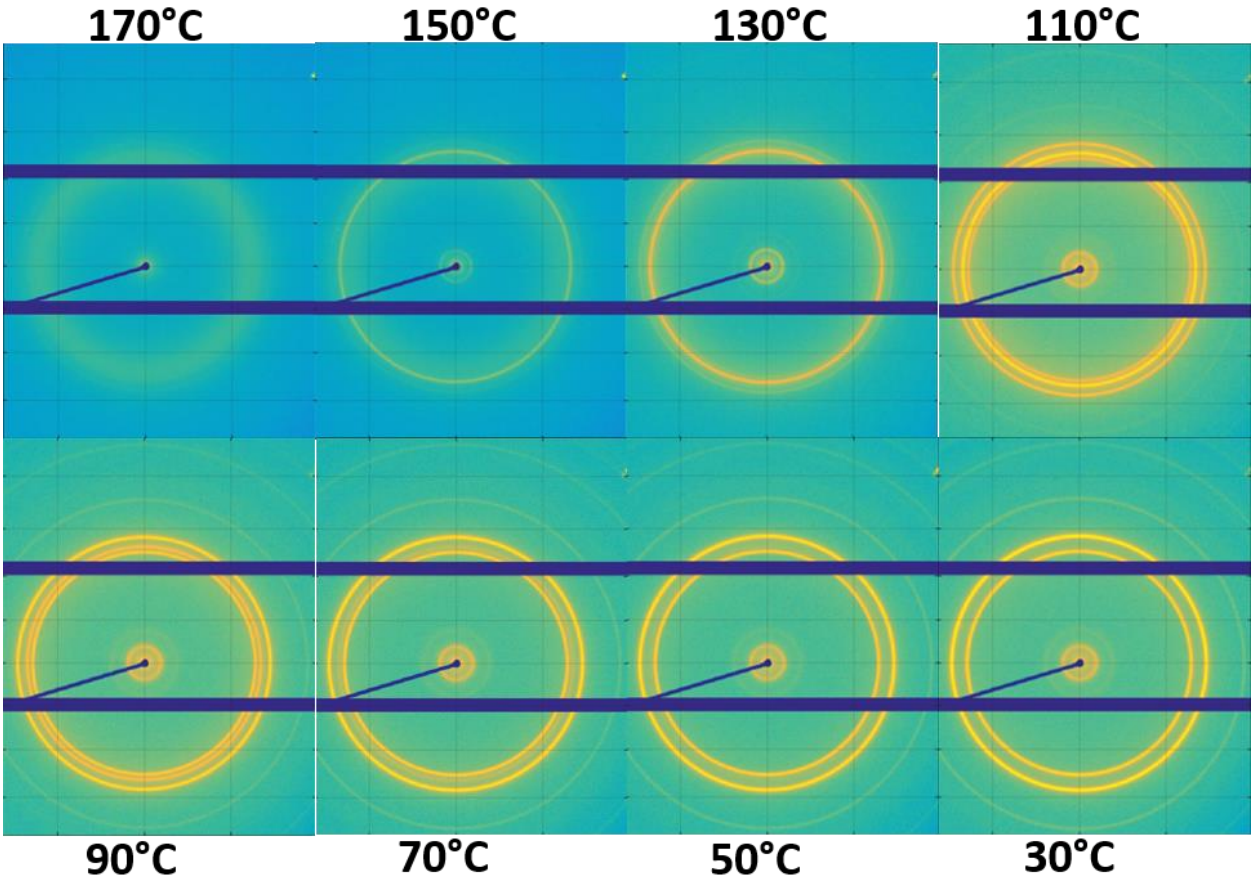

Figure 12A. 2D scattering patterns of crystalline (1,n'-divinyl)oligocyclobutane collected at multiple temperatures.

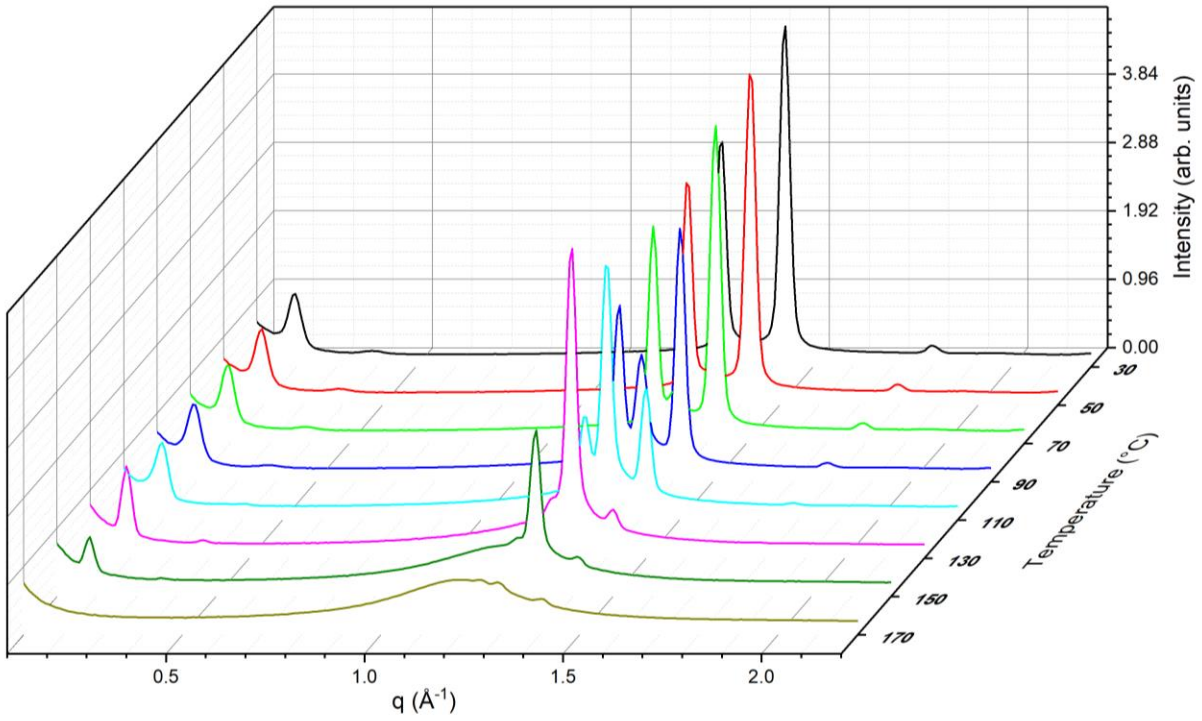

Figure 12B. Masked and reduced 1D scattering curves for crystalline (1,n'-divinyl)oligocyclobutane at varying termperatures.

Data Analysis: Peak fitting was performed in Origin Pro using the Peak Analyzer tool. Initially a strong peak appears as it cools that has been attributed to a transition through a rotator phase as the sample begins to crystallize. The exact nature and stability of this rotator phase has not yet been explored. The peaks were fit using a Levenberg-Marquardt Least-Squares fitting algorithm (Figure 12C). The total area under each set of peaks (attributed to rotator, crystalline, and amorphous fractions respectively) was compared to obtain a relative percent of that phase present at each temperature.

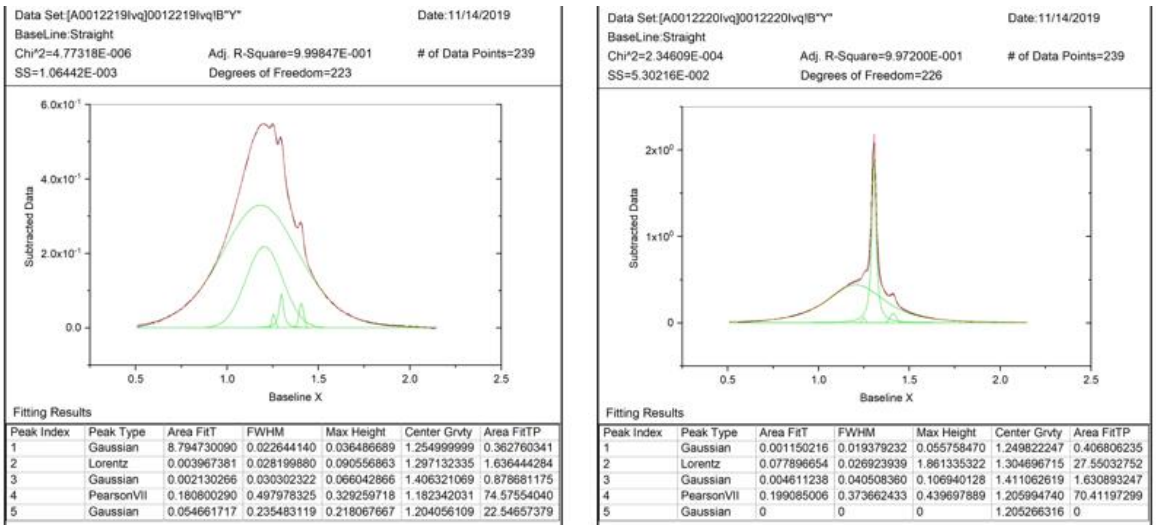

Figure 12C. Peak fitting results for each temperature.

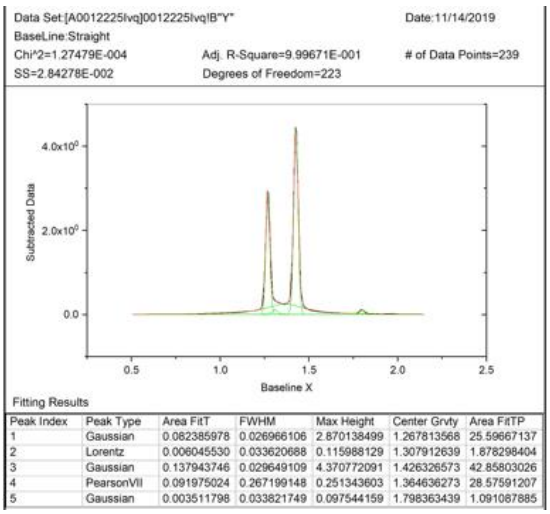

Peak Index	Peak Type	Area FitT	FWHM	Max Height	Center Grvty	Area FitTP
1	Gaussian	0.082385978	0.026966106	2.870138499	1.267813568	25.59667137
2	Lorentz	0.006045530	0.033620688	0.115988129	1.307912639	1.878298404
3	Gaussian	0.137943746	0.029649109	4.370772091	1.426326573	42.85803026
4	PearsonVII	0.091975024	0.267199148	0.251343603	1.364636273	28.57591207
5	Gaussian	0.003511798	0.033821749	0.097544159	1.798363439	1.091087885

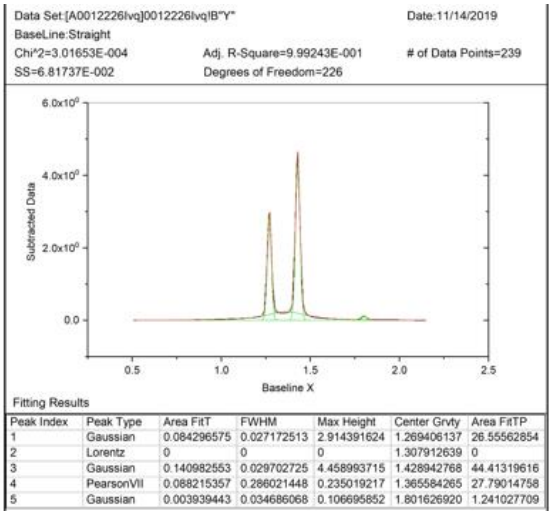

Peak Index	Peak Type	Area FitT	FWHM	Max Height	Center Grvty	Area FitTP
1	Gaussian	0.084296575	0.027172513	2.914391624	1.269406137	26.55562854
2	Lorentz	0	0	0	1.307912639	0
3	Gaussian	0.140982553	0.029702725	4.458993715	1.428942768	44.41319616
4	PearsonVII	0.088215357	0.286021448	0.235019217	1.365584265	27.79014758
5	Gaussian	0.003939443	0.034686068	0.106695852	1.801626920	1.241027709

Figure 12C, continued. Peak fitting results for each temperature.

The calculated phase content is in good agreement with the DSC data. The two exothermic peaks occur at temperatures comparable to the onset of the rotator phase and majority crystal phase transitions (see Figure 12D and Table 7).

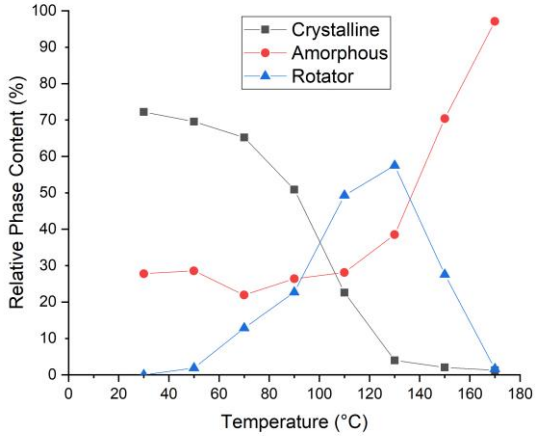

Figure 12D. Relative phase content as a function of temperature of (1,n'-divinyl)oligocyclobutane **(**M_n ~ 973 g mol^{-1}, 17 total cyclobutyls).

Table 7. Relative phase content vs. temperature of (1,n'-divinyl)oligocyclobutane **(**M_n ~ 973 g mol^{-1}, 17 total cyclobutyls).

Temperature (°C)	Crystalline* (%)	Amorphous (%)	Rotator Phase (%)
170	1.2	97.1	1.6
150	2.0	70.4	27.6
130	4.0	38.5	57.5
110	22.6	28.1	49.3
90	50.9	26.4	22.7
70	65.2	21.9	12.9
50	69.5	28.6	1.9
30	72.2	27.8	0.0

MD Simulation of (1,17'-dvinyl)oligocyclobutane Scattering: X-ray scattering simulations for (1,-17')-divinyl-poylcyclobutane were performed using BioVia Materials Studio 2017-R2 based on final coordinates obtained from molecular dynamics (MD) simulations (minimum scattering vector = 0.05 Å, maximum scattering vector = 2.5 Å, scattering atoms cutoff = 75 Å).[9]

Simulations were performed as follows:

1) Observed NMR sequence distributions were used to guide the creation of plausible (1,17'-divinyl)oligocyclobutane oligomer sequences. Low energy conformers were obtained using MacroModel v12.6 (forcefield = OPLS3, search algorithm = Monte Carlo multiple minimum search with low-mode sampling).[1,10-13]

2) Crystalline polymorphs were then generated from the lowest energy molecular mechanics simulated (1,17'-divinyl)oligocyclobutane conformers. Crystalline oligomorphs were generated and screened using Polymorph (forcefield = COMPASSII, fine quality, Ewald sums for van der Waals and electrostatics), as found in BioVia Materials Studio 2017-R2.[4,9-10]

3) 1 ns isothermal/isobaric (NPT) MD simulations on supercells of the crystalline polymorphs were performed using LAMMPS (forcefield = SciPCFF, 12 Å cutoffs, 1 fs time step, triclinic Nose-Hoover thermostat/barostat), as well as a representative amorphous cell created with Scienomics MAPS version 4.3.0.[16-17]

The polymorph which best reproduced the experimental WAXS spectra is a $P2_1$ crystal with the following sequence distribution: *syn-syn-anti-syn-anti-syn-anti-syn-syn-anti-syn-anti-syn-anti-syn-anti-syn* (Figure 13A). The final 30 °C MD equilibrated supercell (3x9x9) featured 87,480 atoms with lattice dimensions of 93.322, 88.451, and 92.019 Å (α = 89.99°, β = 74.96°, γ = 89.99°) (Figure 13B-C). The 170 °C MD equilibrated amorphous cell featured 100 oligomers of the same sequence (18,000 atoms) with final lattice dimensions of 57.410, 60.932, and 59.885 Å (α = 95.72°, β = 89.11°, γ = 89.73°) (Figure S11D). MD coordinate files can be found as supplementary cif files.

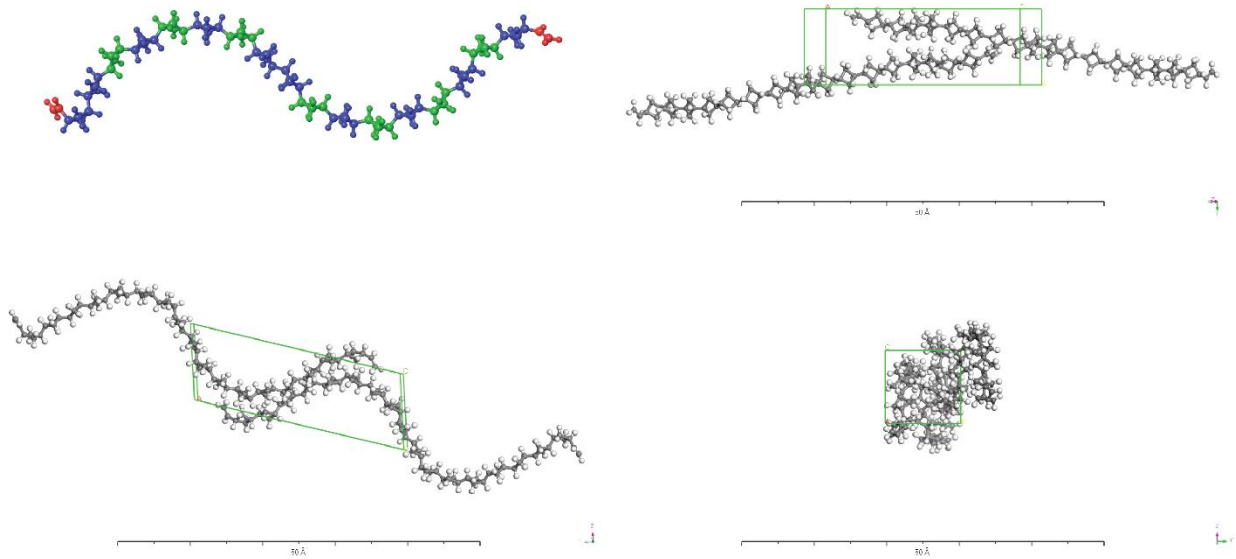

Figure 13A. Representative (1,17'-divinyl)oligocyclobutane (*syn* and *anti* colored blue and green, respectively) and the $P2_1$ crystal used to construct the supercell for MD simulations and X-ray predictions.

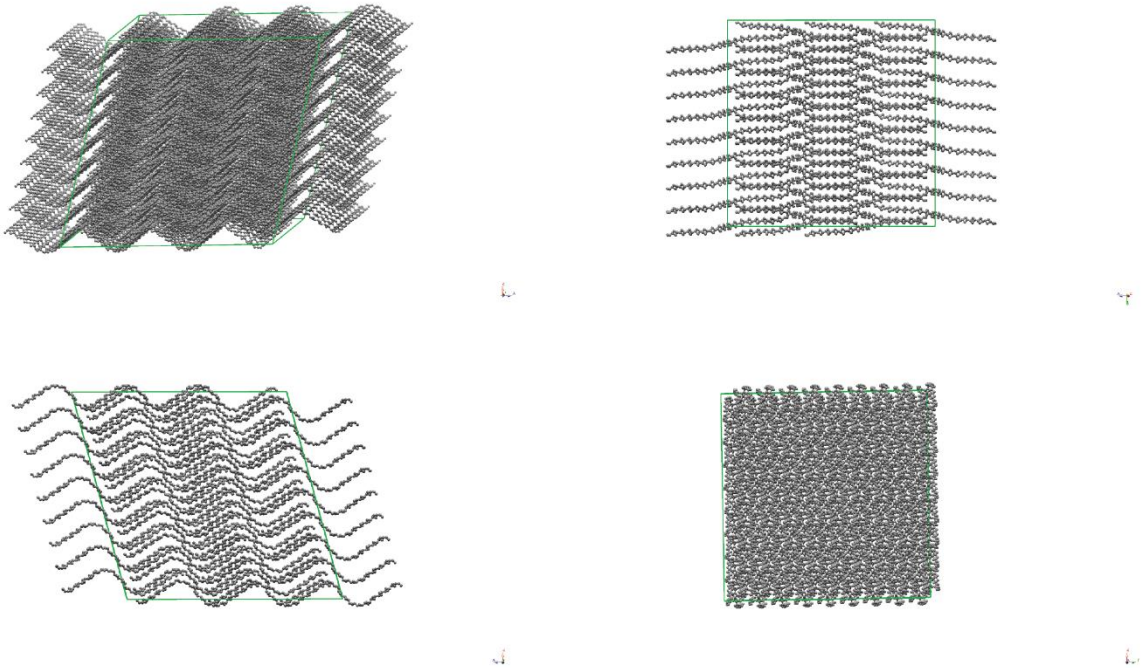

Figure 13B. Final frame of 1 ns MD equilibrated 3x9x9 $P2_1$ supercell used for X-ray predictions colored by element. Hydrogens have been omitted for clarity.

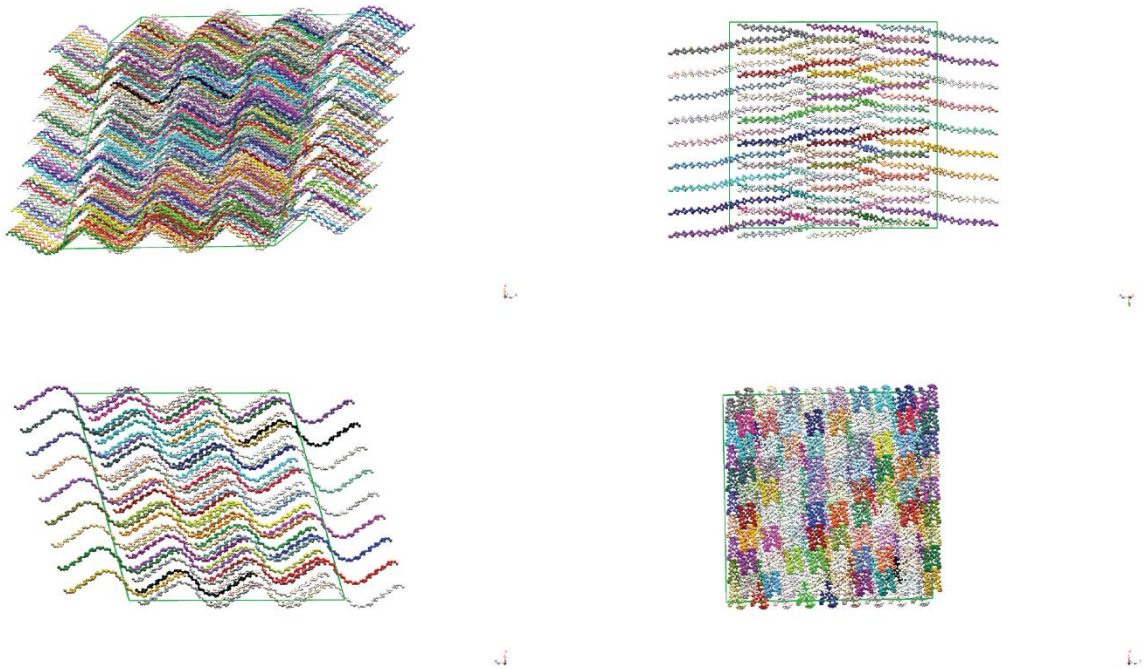

Figure 13C. Final frame of 1 ns MD equilibrated 3x9x9 $P2_1$ supercell used for X-ray predictions colored by molecule. Hydrogens have been omitted for clarity.

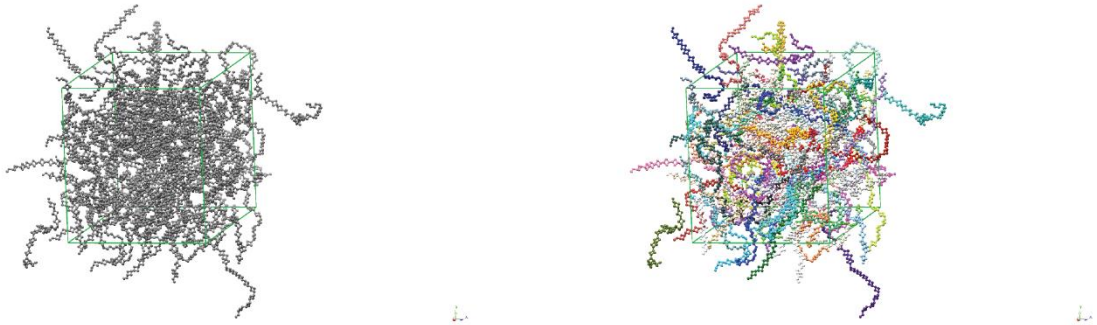

Figure 13D. Final frame of 1 ns MD equilibrated amorphous cell (100 chains) used for X-ray predictions colored by element (left) and molecule (right). Hydrogens have been omitted for clarity.

Simulated scattering of the supercell of (1,17')-dvinyl-oligocyclobutane shows reasonable agreement with the experimental data collected at 30°C and 170°C (Figure 13E).

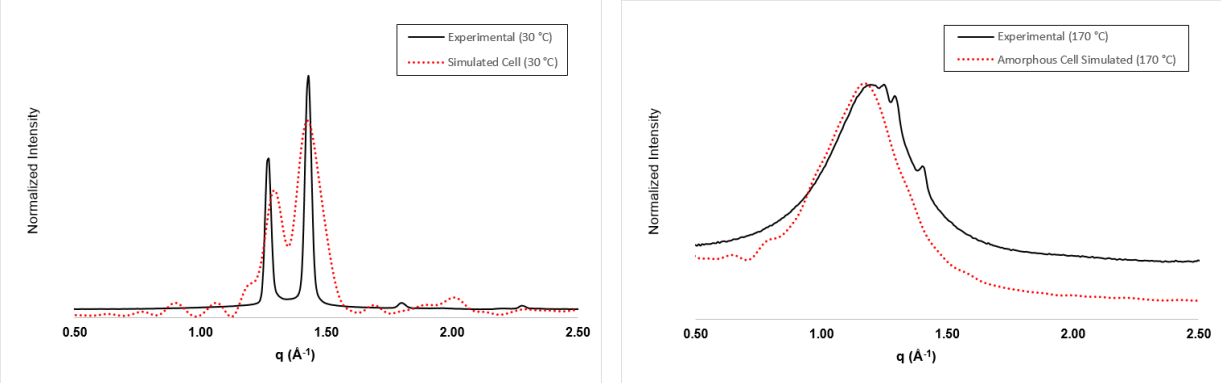

Figure 13E. Experimental WAXS data vs. overlaid with simulated scattering data from MD simulations. Left panel: observed WAXS spectrum of (1,n'-divinyl)oligocyclobutane **(**M_n ~ 973 g mol^{-1}, 17 total cyclobutyls) at 30 °C overlaid with 30 °C molecular dynamics (MD)equilibrated supercell (3x9x9) featured 87,480 atoms with lattice dimensions of 93.322, 88.451, and 92.019 Å (α = 89.99°, β = 74.96°, γ = 89.99°). Right panel: observed WAXS spectrum of (1,n'-divinyl)oligocyclobutane **(**M_n ~ 973 g mol^{-1}, 17 total cyclobutyls) at 170 °C overlaid with MD equilibrated amorphous cell featuring 100 oligomers of the same sequence (18,000 atoms) with final lattice dimensions of 57.410, 60.932, and 59.885 Å (α = 95.72°, β = 89.11°, γ = 89.73°).

VI. Thermal Data

Procedure for the Analysis of (1,n'-divinyl)oligocyclobutane by TGA/GCMS: To a ceramic crucible was added 3.648 mg of (1,n'-divinyl)oligocyclobutane (17 cyclobutyls). The crucible was held at a temperature of 30 °C in an atmosphere of helium in the furnace, after which the material was heated to 700 °C at a rate of 10 °C/min under helium flow. Analysis of weight percent decrease of the material in the crucible as a function of temperature indicated a minor decomposition event at 221 °C, followed by a bulk decomposition event at 413 °C and another minor decomposition event at 476 °C (Figure 14A).

At a sample temperature of 450 °C, the volatiles were diverted to the GCMS instrument and analyzed. GC analysis indicated that the volatiles were composed of one major component. MS (EI+) analysis of the major component revealed a mass corresponding to propyl cation (m/z = 43). Butadiene was not identified in the decomposition mixture, indicating retro-cyclization is not thermally triggered. The gas chromatogram is given in Figure 14B, and the mass spectrum is given in Figure 14C.

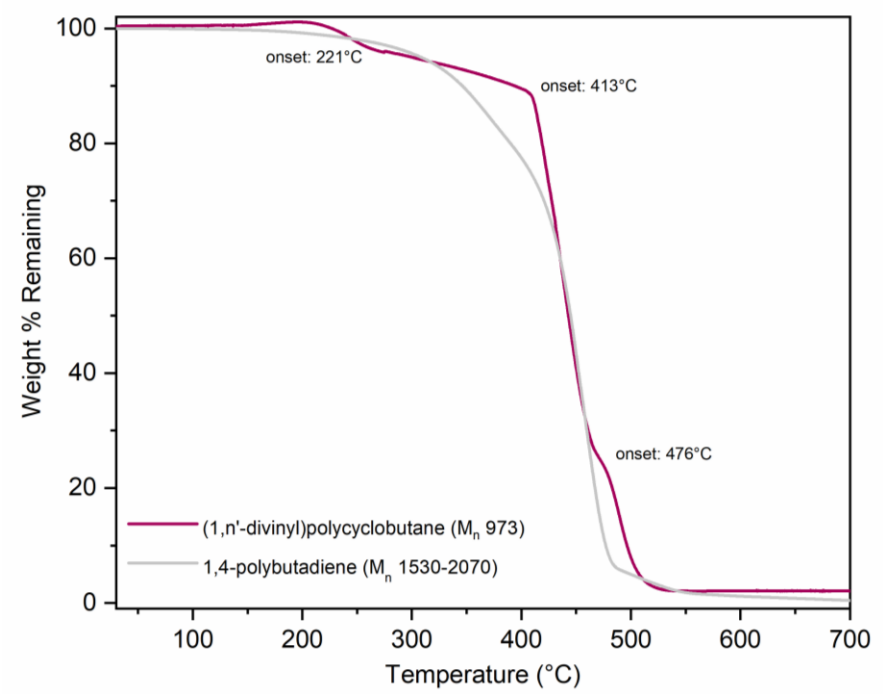

Figure 14A. TGA spectrum for the decomposition of (1,n'-divinyl)oligocyclobutane (M_n ~ 973 g mol^{-1}, 17 cyclobutyls) (maroon). The TGA spectrum of 1,4-polybutadiene (M_n = 1530-2070 g mol^{-1}) is provided for comparison (grey).

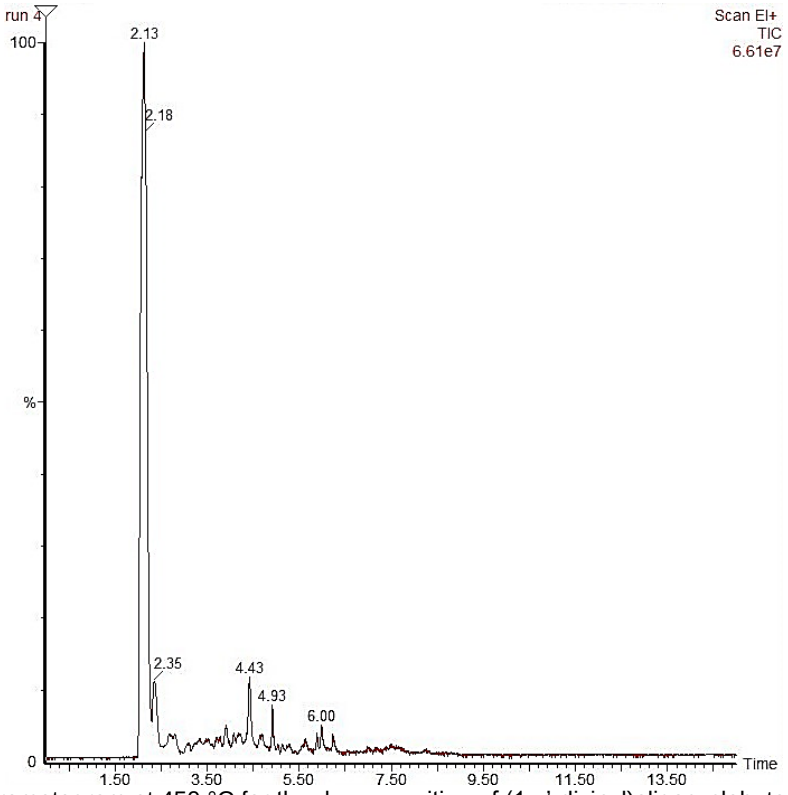

Figure 14B. GC chromatogram at 450 °C for the decomposition of (1,n'-divinyl)oligocyclobutane (M_n ~ 973 g mol^{-1}, 17 cyclobutyls).

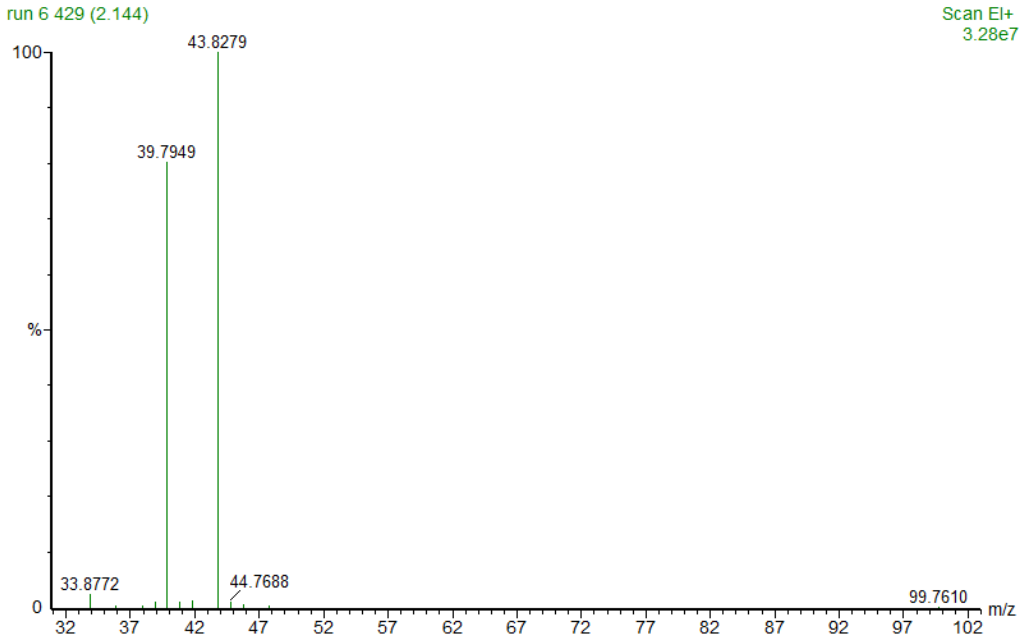

Figure 14C. Mass spectrum for the decomposition product of (1,n'-divinyl)oligocyclobutane (M_n ~ 973 g mol^{-1}, 17 cyclobutyls) occurring at 450 °C and a retention time of 2.13 minutes by GC analysis.

Procedure for the Analysis of (1,n'-divinyl)oligocyclobutane by DSC: To an aluminum pan was added 6.3 mg of (1,n'-divinyl)oligocyclobutane (17 cyclobutyls). The pan was crimp sealed with an aluminum lid. The pan was placed in the DSC oven, using a duplicate empty aluminum pan as a reference. The temperature was cycled in the following sequence: hold at -80 °C for 1 min, ramp from -80 °C to 250 °C at 10 °C/min, hold at 250 °C for 1 min, cool from 250 °C to 30 °C at 25 °C/min, hold at 30 °C for 1 min, ramp from 30 °C to 250 °C at 25 °C/min, hold at 250 °C for 1 min, cool from 250 °C to 30 °C at 25 °C/min. The full DSC spectrum, including isothermal regions, is given in Figure 15.

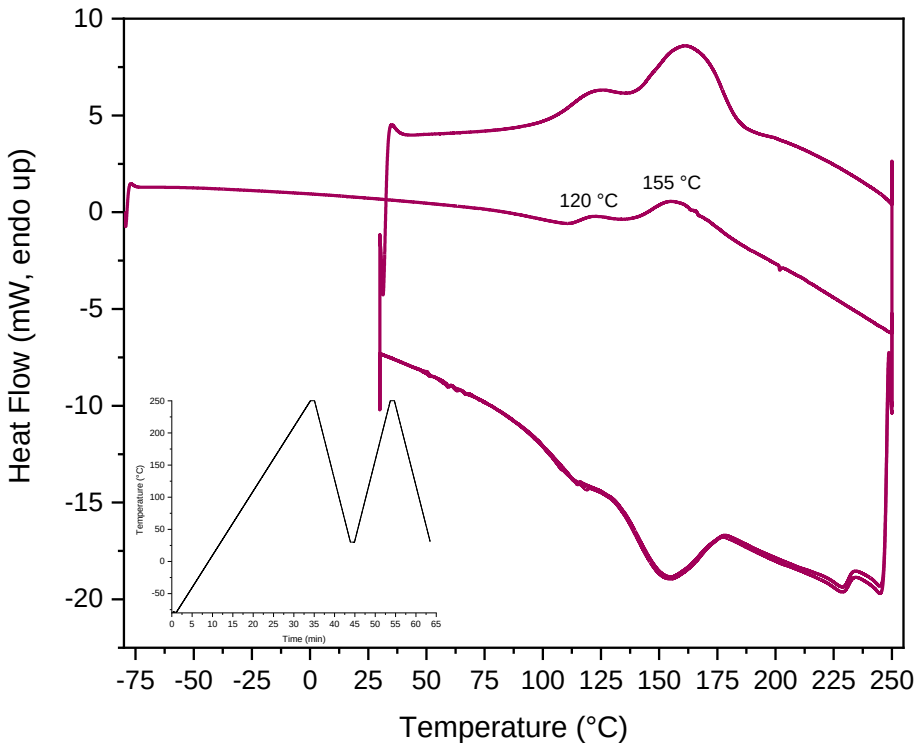

Figure 15. DSC spectrum of the temperature cycling of (1,n'-divinyl)oligocyclobutane (M_n ~ 973 g mol^{-1}, 17 cyclobutyls). Isothermal regions are included. Inset: temperature profile.

Additional DSC data at variable scan rates were acquired on a sample of (1,n'-divinyl)oligocyclobutane oligomer (M_n = 365 g/mol, M_w = 423 g/mol, M_w/M_n = 1.16) using a TA instruments Discovery 25000 differential scanning colorimeter (Figure 16A-D). A TA instruments Tzero, hermetically sealed aluminum pan was utilized with 3.7 mg sample. Estimated peak onset temperatures are shown for thermal transitions. A potential glass transition (T_g) was located at approx. -10 °C. Data analysis was performed with TA instruments TRIOS software.

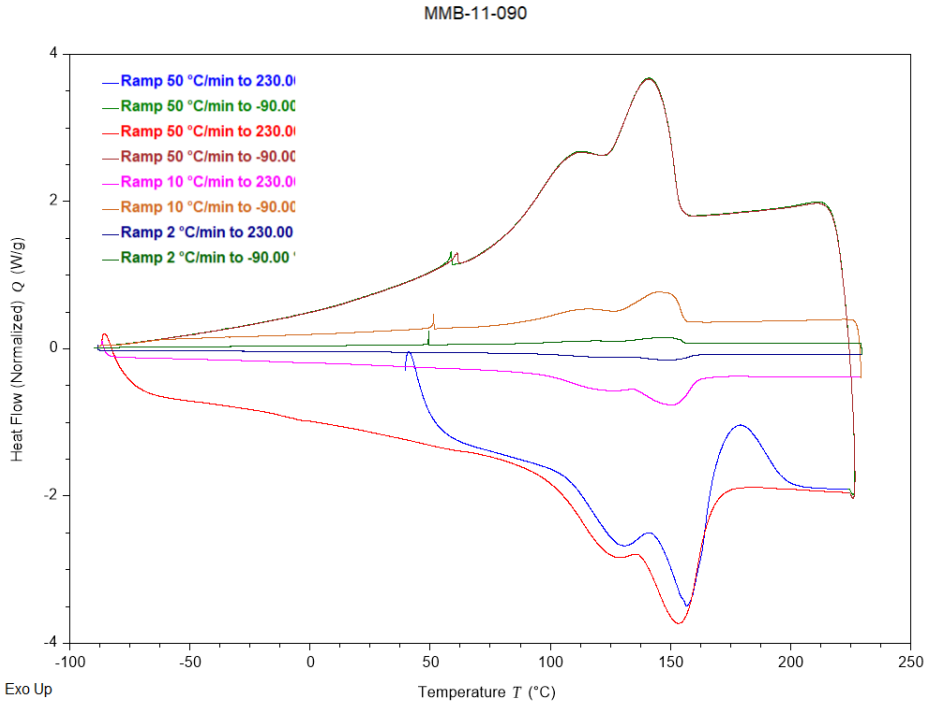

Figure 16A. DSC spectrum of the temperature cycling of (1,n'-divinyl)oligocyclobutane at various scan rates. Experimental sequence listed in legend from top to bottom.

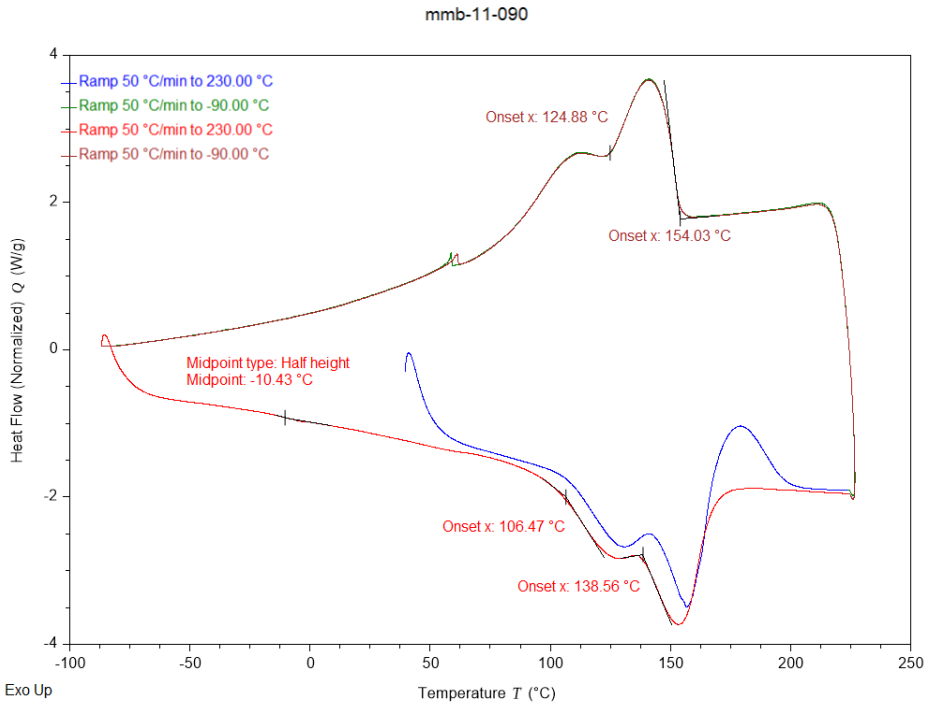

Figure 16B. DSC spectrum of (1,n'-divinyl)oligocyclobutane at a scan rate of 50 °C/min. First and second melt shown. Experimental sequence listed in legend from top to bottom.

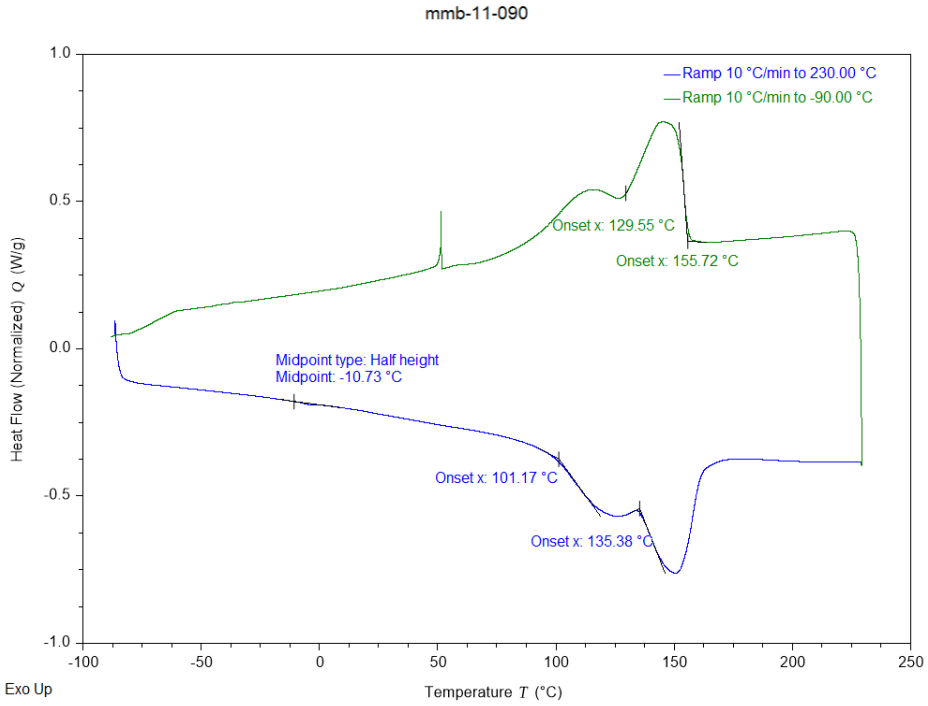

Figure 16C. DSC spectrum of (1,n'-divinyl)oligocyclobutane at a scan rate of 10 °C/min. Experimental sequence listed in legend from top to bottom.

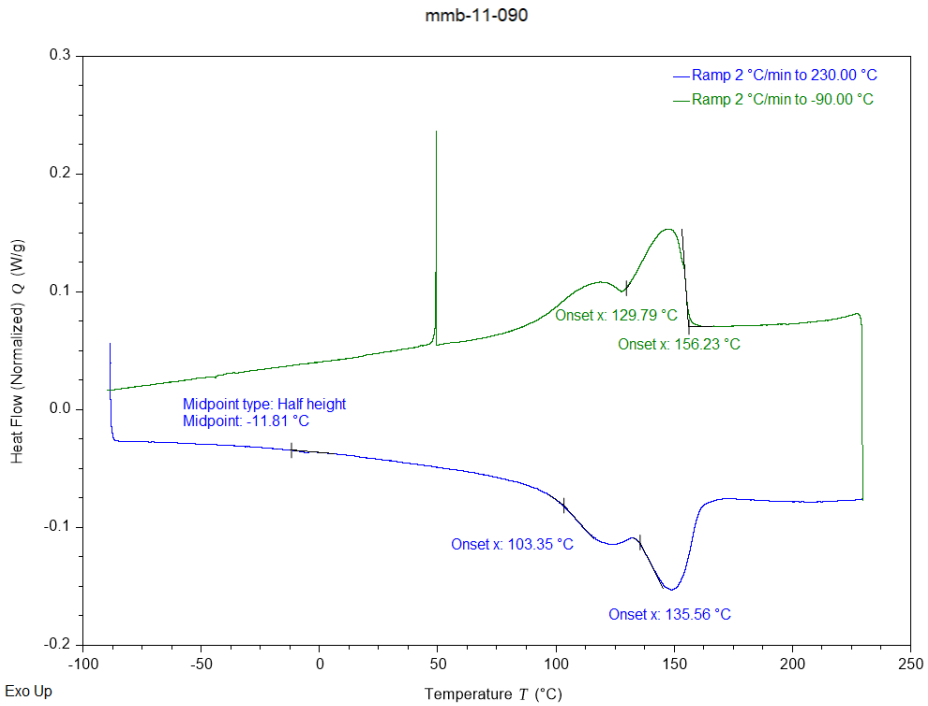

Figure 16D. DSC spectrum of (1,n'-divinyl)oligocyclobutane at a scan rate of 2 °C/min. Experimental sequence listed in legend from top to bottom.

Comparative DSC Data for Hydrogenated vs. Native Oligomer: Second melt DSC data are presented for (1,n'-divinyl)oligocyclobutane (M_n ~ 581 g/mol, ~10 cyclobutyls) before and after hydrogenation (Figure 17A and 17B, respectively). Small shifts in the thermal peaks are observed but major thermal features remain unchanged.

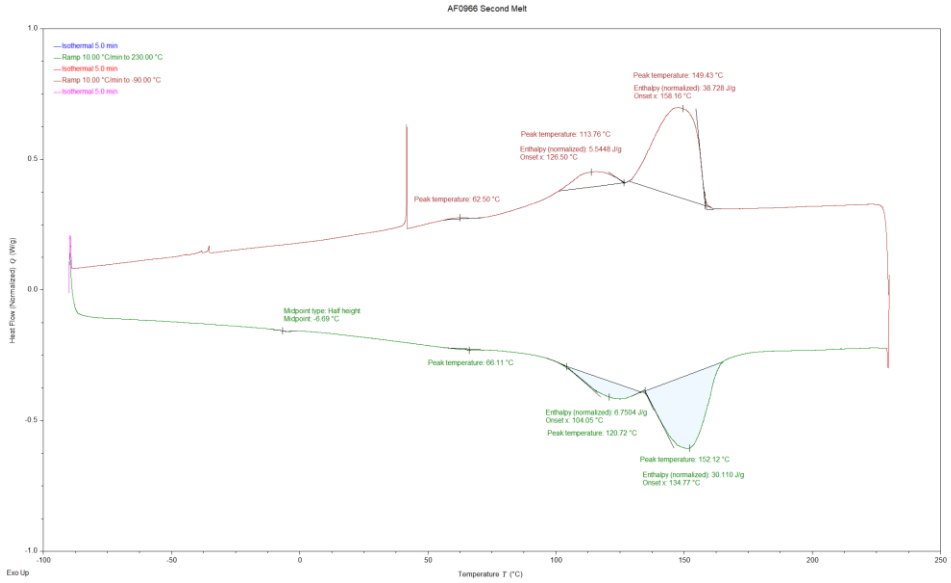

Figure 17A. DSC spectrum of (1,n'-divinyl)oligocyclobutane (M_n ~ 581 g/mol, ~10 cyclobutyls) at a scan rate of 10 °C·min^{-1}. Experimental sequence listed in the legend from top to bottom.

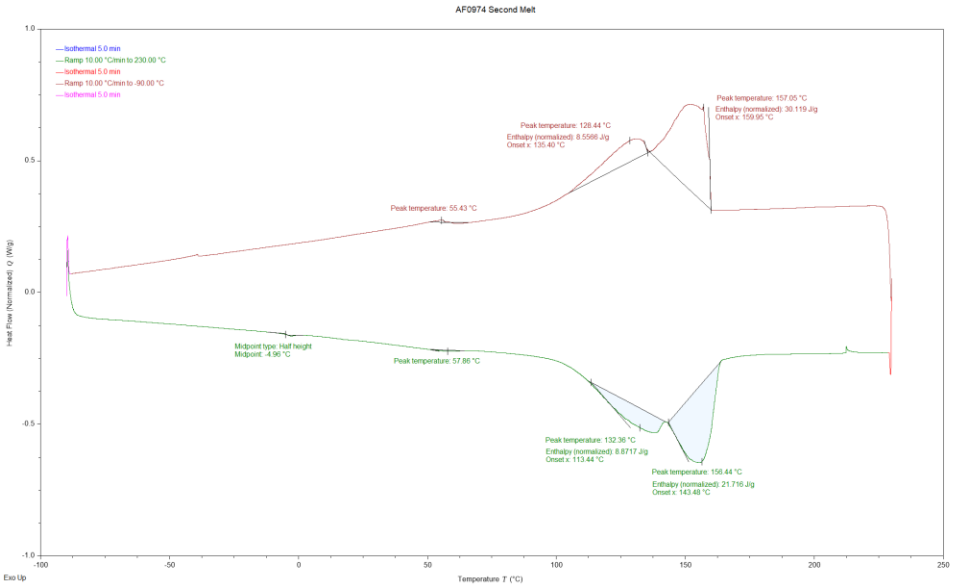

Figure 17B. DSC spectrum of (1,n'-diethyl)oligocyclobutane (M_n ~ 599 g mol^{-1}, 10 cyclobutyls) at a scan rate of 10 °C·min^{-1}. Experimental sequence listed in the legend from top to bottom.

Procedure for the Analysis of Oxidative Induction Time: The oxidative stability of (1,n'-divinyl)oligocyclobutane (M_n ~ 581 g/mol, ~10 cyclobutyls, and hydrogenated (1,n'-divinyl)oligocyclobutane was investigated by DSC. In this experiment the sample was brought to 200 °C under a nitrogen atmosphere and equilibrated. At time = 0 the atmosphere was purged with oxygen (40 mL/min) at and the induction time before oxidation (as measured by heat flow) measured) (Figure 18A and 18B). Both samples underwent rapid oxidation with the hydrogenated material, (1,n'-diethyl)oligocyclobutane, requiring slightly longer to fully oxidize.

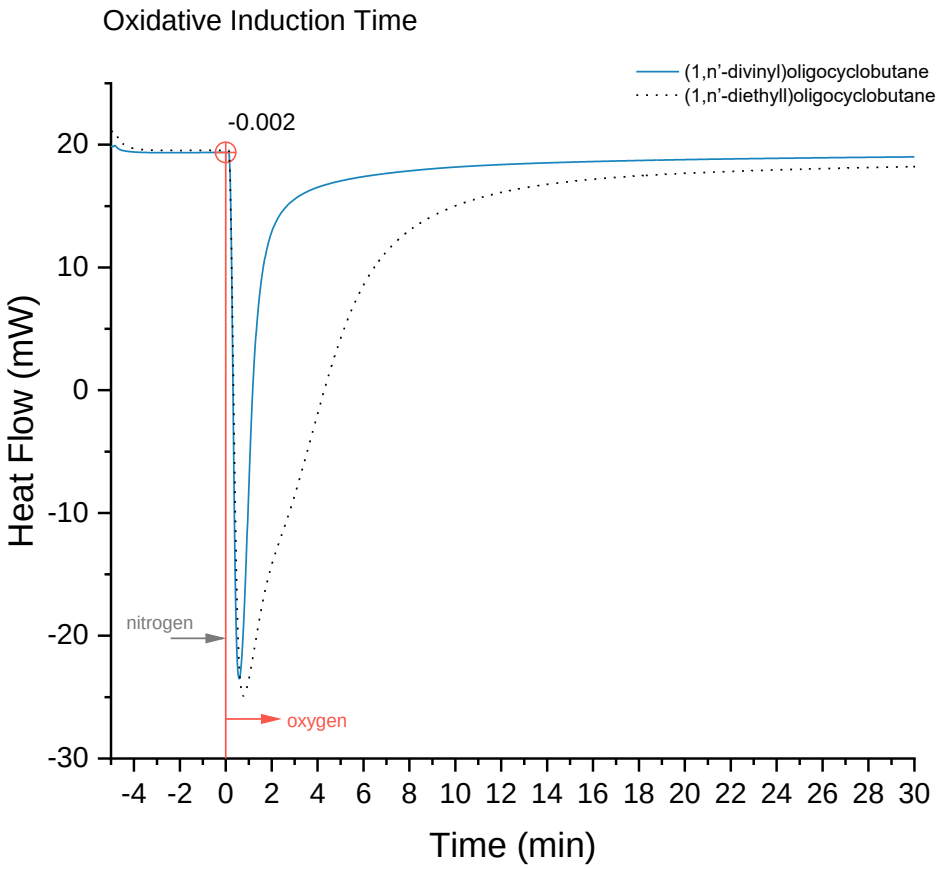

Figure 18A. Plot of time (min) versus heat flow (mW) for oxidative induction time testing. Results for (1,n'-divinyl)oligocyclobutane and (1,n'-diethyl)oligocyclobutane are shown. The red line marks T=0 when the atmosphere was purged with oxygen (40 mL/min).

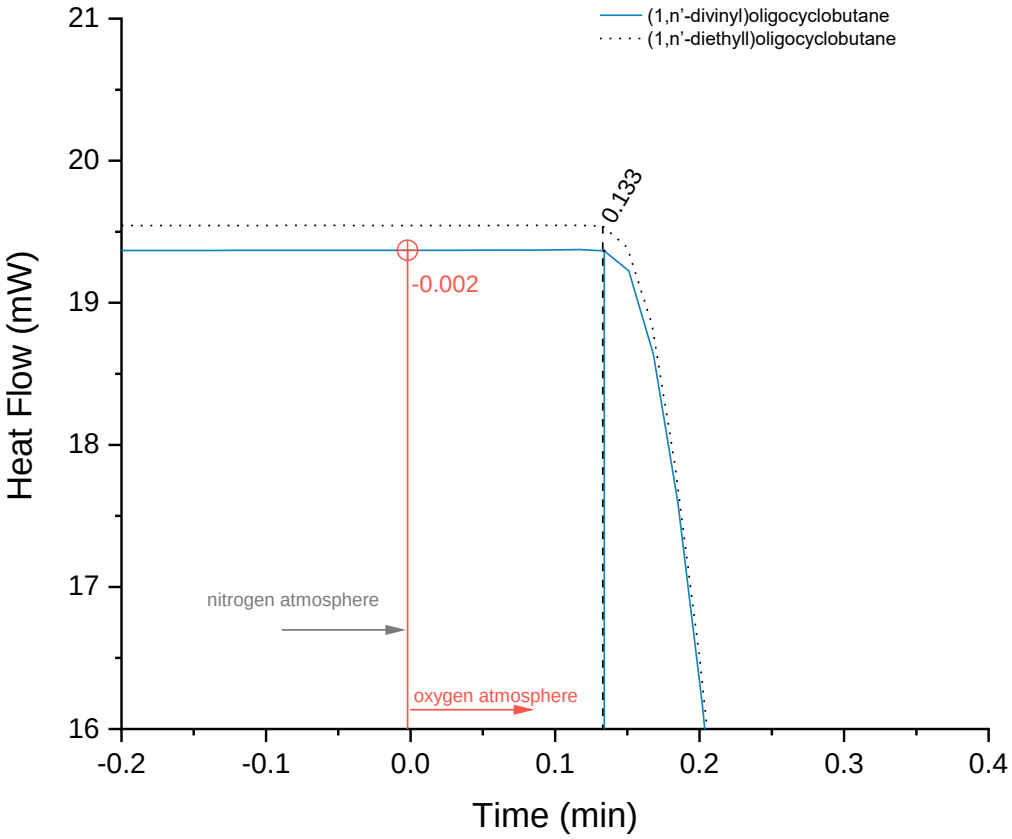

Figure 18B. Enlarged plot of time (min) versus heat flow (mW) for oxidative induction time testing. Results for (1,n'-divinyl)oligocyclobutane and (1,n'-diethyl)oligocyclobutane are shown. The red line marks T=0 when the atmosphere was purged with oxygen (40 mL/min). The onset of oxidation is marked at t = +0.133 min.

VII. Chemical Recycling of Cyclobutane Structures

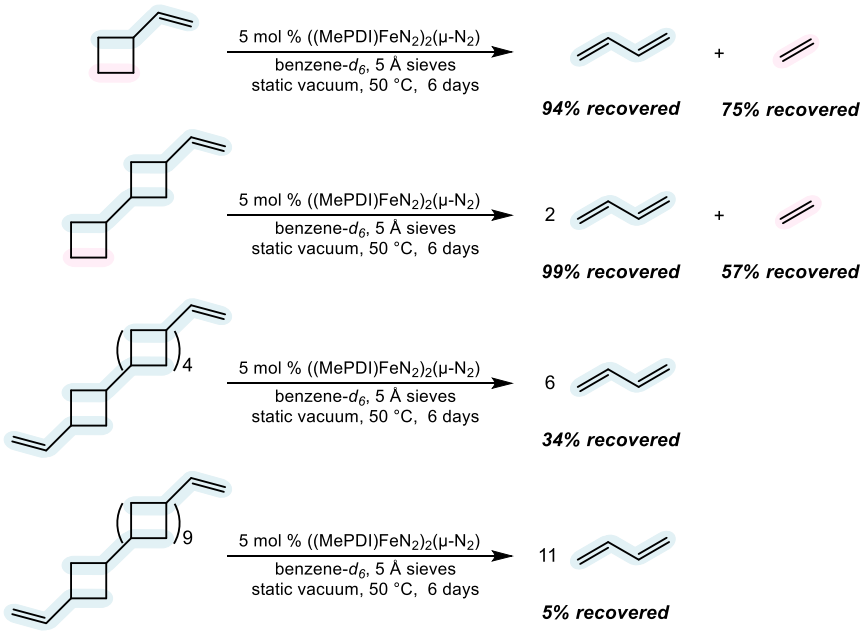

Spectroscopic Data for Chemical Recycling of Cyclobutane Structures: The spectra for the decomposition of vinylcyclobutane, 3-vinyl-1,1'-dicyclobutane, (1,5'-divinyl)oligocyclobutane (5 cyclobutyl rings), and (1,10'-divinyl)oligocyclobutane (10 cyclobutyl rings) are given in Figure 19A, 19B, 19C, and 19D, respectively. Over several iterations, recovered yields of ethylene and butadiene ranged from ~ 40 – 99% for the decomposition of vinylcyclobutane and 3-vinyl-1,1'-dicyclobutane, and from ~5 – 34% for the decomposition of oligomers. This variability is attributed to the variations in experimental setup, including vacuum transfer of materials post-deoligomerization.

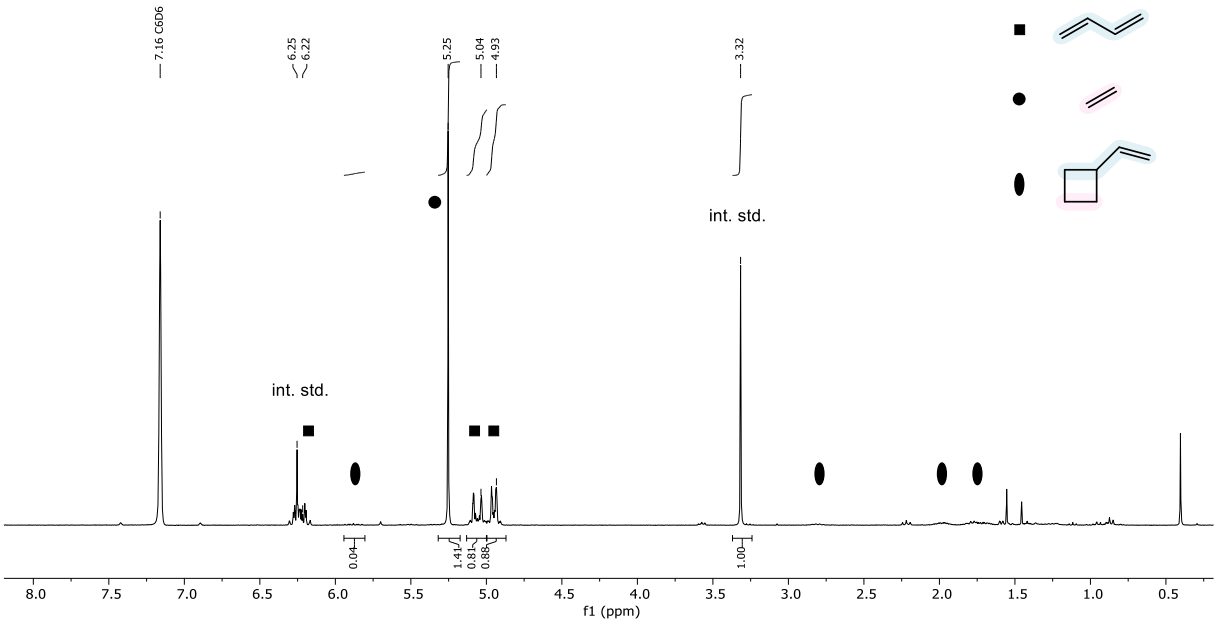

Figure 19A. ^{1}H NMR (300 MHz, benzene-d_6, 25 °C) spectrum of the volatile products formed from the catalytic decomposition of vinylcyclobutane.

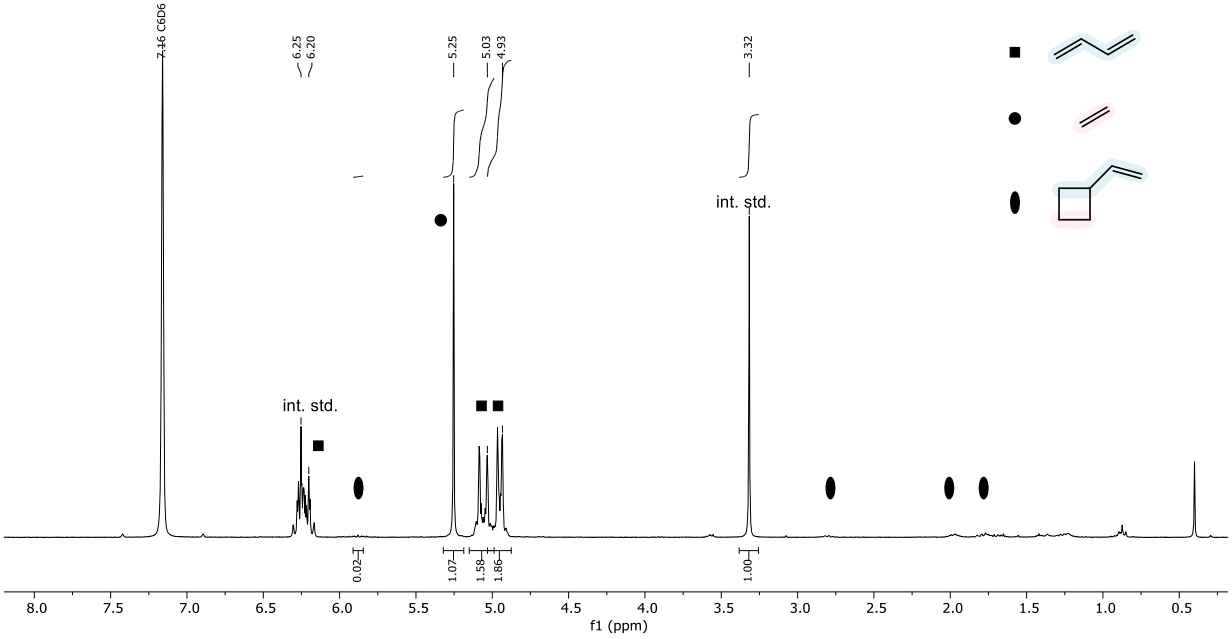

Figure 19B. ^{1}H NMR (300 MHz, benzene-d_6, 25 °C) spectrum of the volatile products formed from the catalytic decomposition of 3-vinyl-1,1'-dicyclobutane.

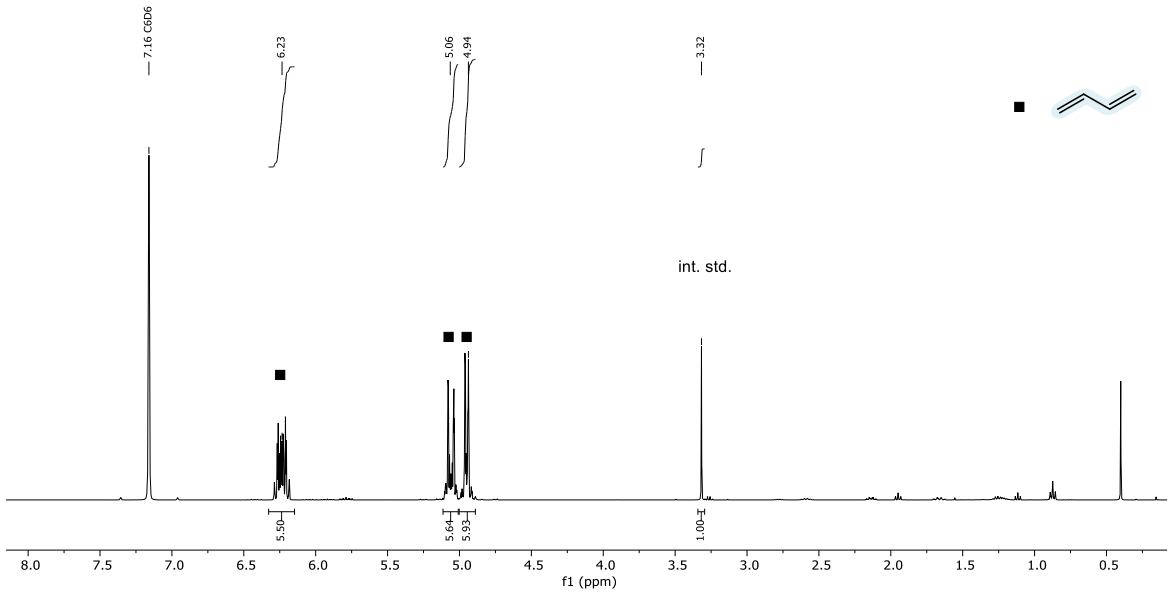

Figure 19C. ^{1}H NMR (300 MHz, benzene-d_6, 25 °C) spectrum of the volatile products formed from the catalytic decomposition of (1,5'-divinyl)oligocyclobutane (5 cyclobutyl rings).

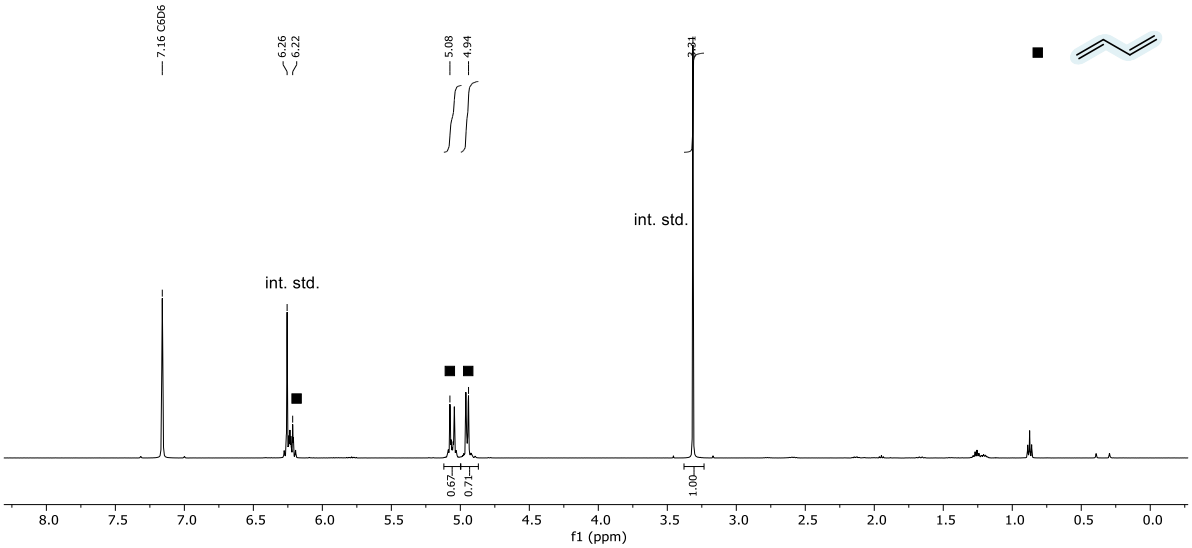

Figure 19D. ^{1}H NMR (500 MHz, benzene-d_6, 25 °C) spectrum of the volatile products formed from the catalytic decomposition of (1,10'-divinyl)oligocyclobutane (10 cyclobutyl rings).

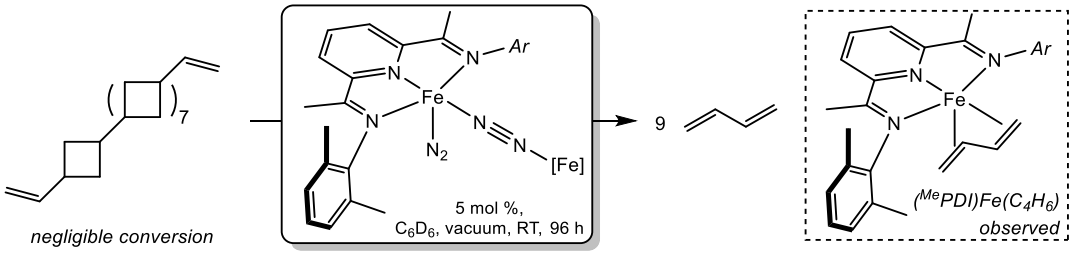

Monitoring of (1,n'-divinyl)oligocyclobutane Deoligomerization by ^{1}H NMR: In a vial in a glove box was added 45 mg (0.0924 mmol) of (1,n'-divinyl)oligocyclobutane (8 total cyclobutyls) and 4 mg (0.00462 mmol, 0.05 equiv.) of $(({}^{Me}PDI)FeN_2)_2(\mu\text{-}N_2)$. The reactants were taken up in 500 µL of benzene-d_6 and added to a J Young tube. The tube was sealed, and an initial ^{1}H NMR was immediately taken. The tube was then frozen in liquid nitrogen, and the headspace evacuated on a high vacuum line. The tube was thawed, and another ^{1}H NMR was immediately taken. The tube was then agitated by inversion for 4 days, with ^{1}H NMR spectra taken intermittently (Figure 20). Analysis of the reaction mixture by ^{1}H NMR indicates that $({}^{Me}PDI)Fe(C_4H_6)$ is formed over the course of several hours and persists as the dominant iron species in solution over several days, coinciding with little to no consumption of oligomer or release of free butadiene. This implies that coordination of butadiene to the active iron catalyst is inhibitory to the deoligomerization process and thus increased temperatures and molecular sieves are needed to sequester butadiene from the iron catalyst.

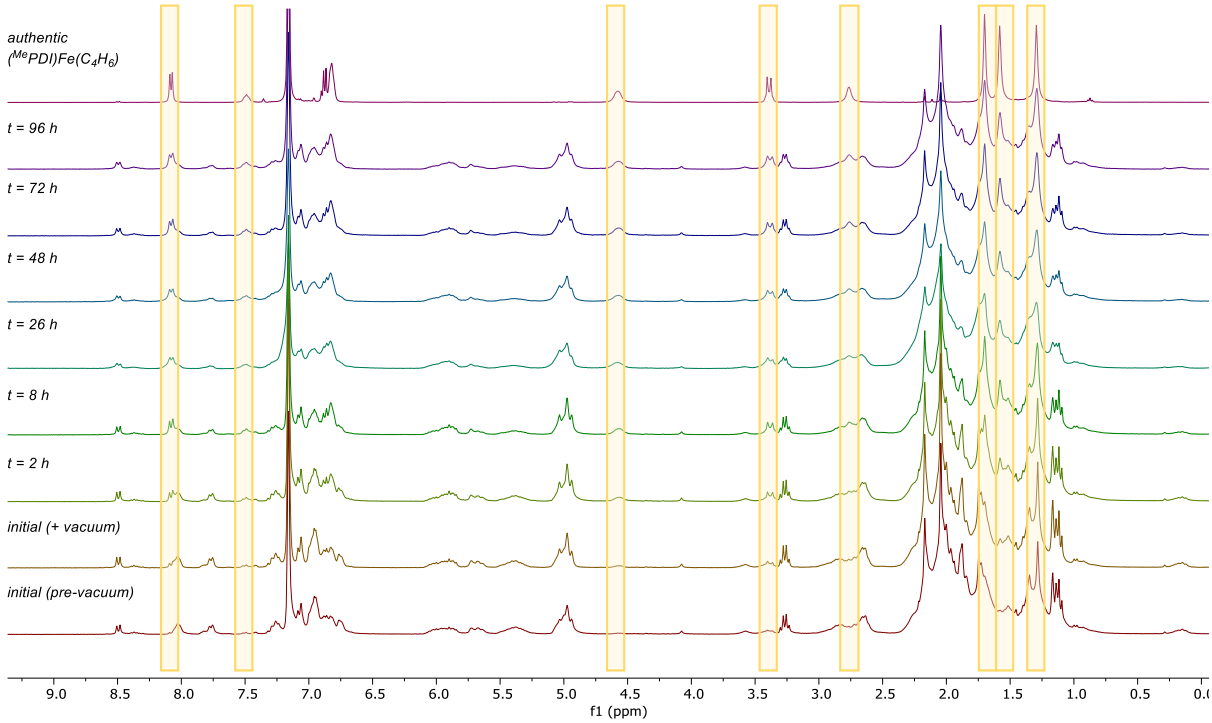

Figure 20. ^{1}H NMR (300 MHz, benzene-d_6, 25 °C) time course of iron-mediated deoligomerization of (1,n'-divinyl)oligocyclobutane. An authentic spectrum of (^{Me}PDI)Fe(C_4H_6) (top) is provided for comparison.

VIII. Gelation Test

Procedure for Gelation Test: A medium-sized Soxhlet apparatus equipped with Allihn condenser, extractor, boiling flask (500 mL) and PTFE coated stir bar was charged with *para*-xylene (300 mL). A tared extraction thimble (18.9427 g; course porosity fritted glass) was charged with a sample of dry, (1,n'-divinyl)oligocyclobutane (M_n ~ 595 g/mol, ~10 cyclobutyls, 1.0417 g) and loaded into the extractor. The sample was subjected to continuous extraction for 16 h under a dinitrogen atmosphere. After 16 h, the apparatus was cooled and opened. Only a small quantity of brown-residue remained. It was then dried at 150 °C for 1 h and then weighed.

	Mass (g)
Mass thimble + sample (pre-extraction)	19.9844
Mass thimble (dry)	18.9427
Mass sample (calcd.)	1.0417
Mass thimble + residue (post-extraction)	18.9658
Mass thimble (dry)	18.9427
Residue Mass (calcd.)	0.0231
% Mass Insoluble	2.22%

IX. DFT Simulation of Reaction Free Energies

RKS Calculations of the Full Reaction Profile: Reaction energies were calculated using components found within Schrödinger Materials Science Suite Release 2019-4, 2020-1 and 2020-2. Up to five low energy conformers were considered as starting points per stationary point (MacroModel v12.6, forcefield = OPLS3, search algorithm = Monte Carlo multiple minimum search with low-mode sampling).[10-12,18] Density functional theory calculations followed using Jaguar v10.6 release 12.[1] Singlet geometries were optimized with the B3LYP-D3, M06-L, and TPSSh functionals and the LACVP** basis set.[19-22] LACVP features an effective core potential for iron and a 6-31G Pople basis for all other atoms. Additional higher energy single points were calculated at LACV3P**+, with and without implicit solvent models CPCM (conductor-like polarizable continuum model) and SM8 (decane as the solvent).[23-24] LACV3P is the triple-zeta contraction of the LACVP basis set. Additional diffuse (+) and polarization (*) functions follow standard conventions. Vibrational mode analysis confirmed minima and saddle points. Energies are given as the Boltzmann ensemble at the appropriate temperature.

Substantial overestimation of entropic contributions excludes the use of free energy differences (ΔG) in energy landscape analysis, as such, energy differences were calculated without the problematic entropy (and internal energies) by using only the self-consistent field energy (SCFE) plus the zero-point energy (ZPE) (Figure 21).[25] These energy differences yield reasonable barriers of 20-25 kcal/mol, as well as a small negative energy of formation. The overestimation of entropy and internal energy at 50 °C and 1 atm is very large at 22 +/- 7 kcal/mol across all stationary points, functionals, and solvation models. All results are consistent and can be found in supplementary Excel file. DFT coordinate files (and energies) can be found as supplementary mae files.

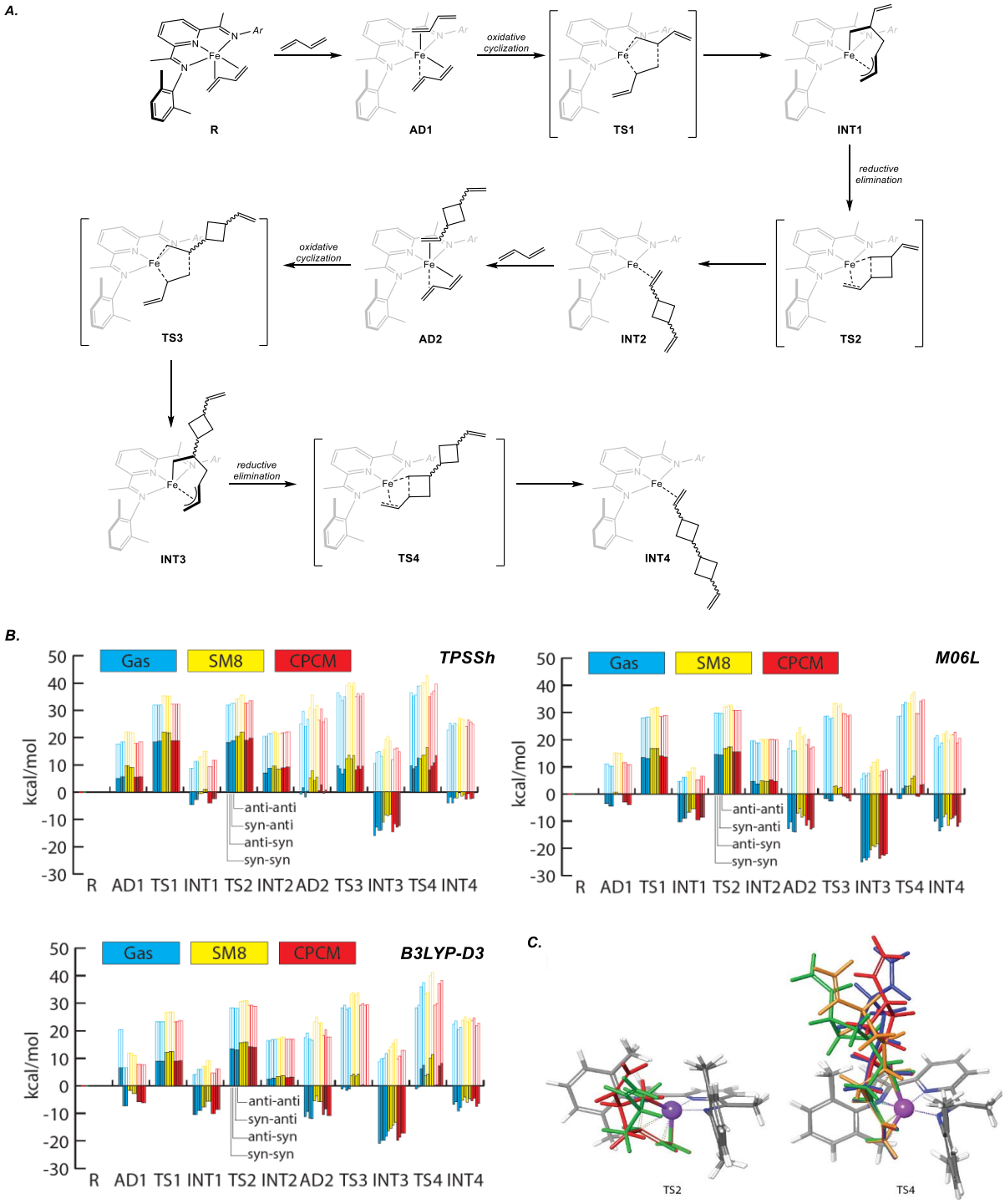

Figure 21. DFT/TST results for growth of (1,n'-divinyl)oligocyclobutane as catalyzed by (MePDI)Fe at LACV3P**+//LACVP**. **A.** Naming scheme for intermediates and transition states. **B.** Energy differences Δ(E+ZPE) [foreground] and ΔG [background] at LACV3P**+//LACVP** (50 °C and 1 atm) for stationary points in the reaction cycle relative to reactants with three different solvent models: SM8, CPCM and gas phase. **C.** Select optimized geometries for rate determining steps 1st (TS2) and 2nd (TS4) [2+2]-cycloaddition.

Evaluation of Other Spin Manifolds: Stationary points were screened at Kohn-Sham restricted (RKS), unrestricted (UKS) and broken-symmetry (BS) stationary points. In broken-symmetry notation, BS(*m,n*) describes a state where there are *m* unpaired spin up electrons and *n* unpaired spin down electrons on separate fragments. For example, to obtain a BS(3,1) triplet state where there are three unpaired up spins on the ferric iron (site A) antiferromagnetically coupled to one unpaired down spin on the reduced ligand (site B), first the complex was optimized as an unrestricted high-spin quartet, in other words UKS(S=4). Second, the highest virtual ligand orbital and highest occupied iron orbital are swapped in the input basis guess and the resulting spin densities of the converged triplet self-consistent field calculation checked to ensure a ferric iron and a reduced ligand. An analogous procedure was followed to generate the BS(1,1) singlet state starting from the optimized UKS(S=1) triplet. The results from these calculations are labeled as BS(3,1)//UKS(S=4) and BS(1,1)//UKS(S=1) signifying a single-point at the optimized high-spin unrestricted geometry. Further, these BS single points were used as starting points for additional geometry optimizations along the BS spin manifold (e.g. BS(3,1)//BS(3,1)).

Both UKS and BS suffer from spin contamination. For the latter, the spin contamination is substantial because the BS electronic state is not an eigenfunction of the single determinant spin Hamiltonian, therefore the absolute value of the energy is suspect. The Yamaguchi spin-projection approach is used to obtain the spin-projected energies given the following spin Hamiltonian[26,27]:

$$H = -2J\hat{S}_A\hat{S}_B$$

The value of the exchange coupling constant *J* can be approximated from the energies and spin expectation values of the of the high-spin and broke-symmetry states (at the given geometry):

$$J = -\frac{E_{HS} - E_{BS}}{\langle\hat{S}^2\rangle_{HS} - \langle\hat{S}^2\rangle_{BS}}$$

If J <0, than the BS state is higher in energy than the true antiferromagnetic multi-determinant state (Table 8). The following spin ladder is then used to approximate the energy of the multi-determinant state:

$$E(S-1) = E(S) + 2JS; S = S_A + S_B$$

Table 8. Exchange coupling constants at TPSSh/LACV3P**+//LACVP** at 50 °C and 1 atm in cm^{-1}. J<0: Antiferromagnetic coupling. J>0: Ferromagnetic coupling. RKS: geometry optimization of the BS(1,1) state which converged to the restricted solution.

	BS(1,1)//UKS(S=1)	BS(1,1)//BS(1,1)	BS(3,1)//UKS(S=4)	BS(3,1)//BS(3,1)
R	-208	-606	-1420	-1847
syn-AD1	-304	*RKS*	-247	-2060
anti-AD1	647	208	-290	-1171
syn-TS1	-98	*RKS*	-934	-3366
anti-TS1	-40	*RKS*	-864	-2948
syn-INT1	130	*RKS*	-2275	-3026
anti-INT1	537	*RKS*	-2315	-2921
syn-TS2	-528	*RKS*	-1472	-2378
anti-TS2	647	*RKS*	-1322	-1903
syn-INT2	1651	-413	-476	-1328
anti-INT2	1675	-491	-321	-1246
syn-syn-AD2	-320	*RKS*	-1174	-1559
anti-syn-AD2	-68	-377	374	-5652
syn-anti-AD2	-256	*RKS*	-293	-1254
anti-anti-AD2	762	-406	-451	-1310
syn-syn-TS3	-150	90	-1887	-2901
anti-syn-TS3	-171	*RKS*	-2665	-4091
syn-anti-TS3	-105	*RKS*	-4271	2530
anti-anti-TS3	-220	*RKS*	-2140	-2013
syn-syn-INT3	536	*RKS*	-5782	-3023
anti-syn-INT3	558	235	-2358	-4070
syn-anti-INT3	184	*RKS*	-2695	-2888
anti-anti-INT3	-787	*RKS*	-2372	-2841
syn-syn-TS3	-150	90	-1887	-2901
anti-syn-TS4	-171	*RKS*	-2665	-4091
syn-anti-TS4	-1928	-1444	-1557	-1756
anti-anti-TS4	-192	-854	-1357	-1476
syn-syn-INT4	1592	-356	-493	-902
anti-syn-INT4	1321	-529	-348	-1875
syn-anti-INT4	1445	-600	-380	-1879
anti-anti-INT4	1521	-578	-526	-1644

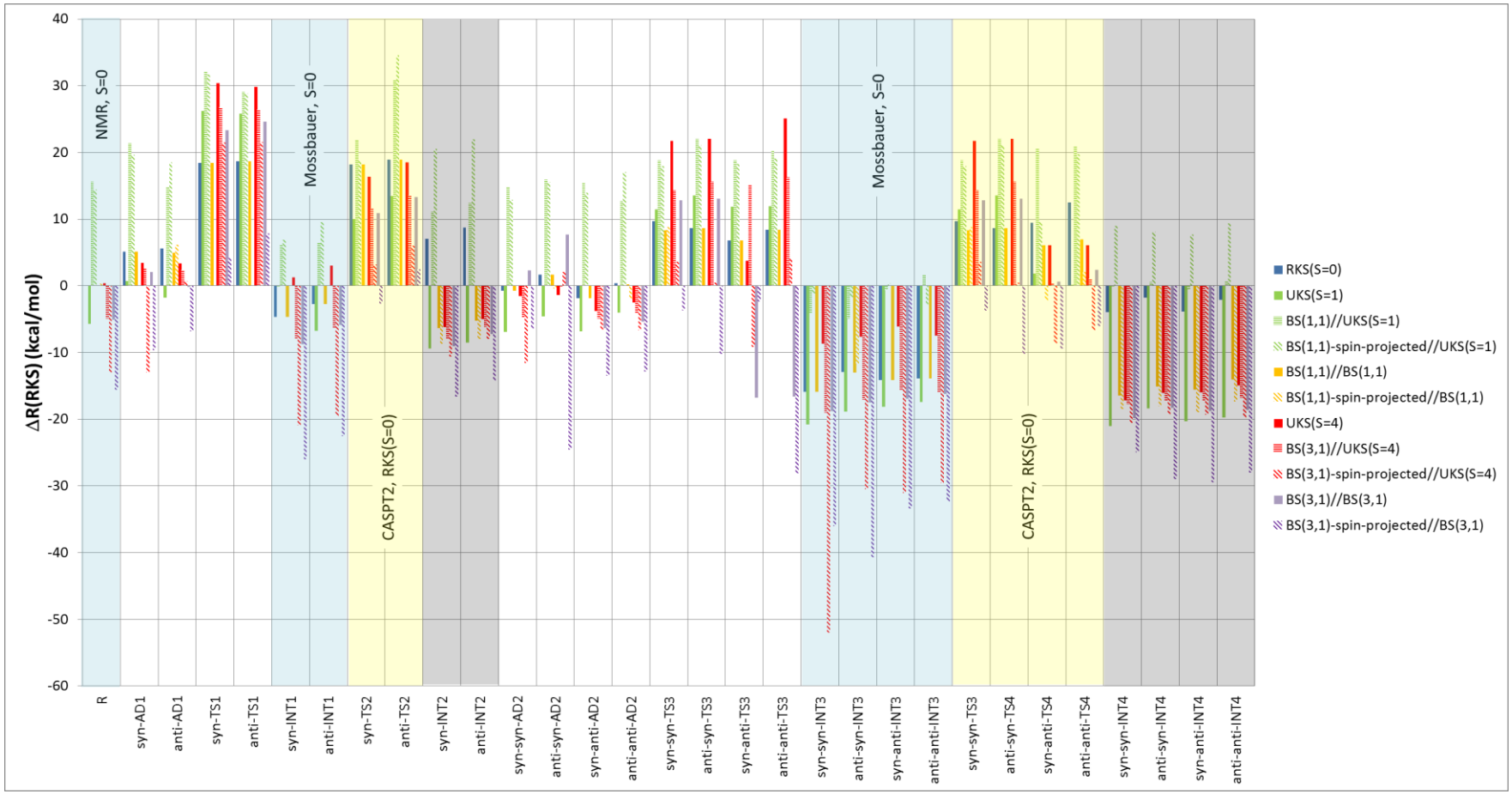

Figure 22. TPSSh/LACV3P**+//LACVP** RKS, UKS, and BS energies (E+ZPE) relative to the RKS reactants at 50 °C and 1 atm. Sections highlighted in blue represent species which are best represented as restricted singlets from experiment: NMR (this work), Mossbauer.[28] Sections highlighted in yellow are best represented as restricted singlets from the results of CASPT2 calculations.[29] Sections highlighted in gray are 16-electron stationary points with near zero populations.[28,30]

RKS, UKS, BS, and spin-projected BS energies, relative to RKS reactants (R) are graphed in Figure 22. Also shown is where the electronic state of the complex (or an analogous 18-electron Fe-PDI metallocycle) have been experimentally characterized by NMR and Mossbauer (e.g. reactant, INT1, and INT3).[28] Minimum-energy crossing point and multireference CASPT2 calculations by Chen tested the probability of two-state reactivity for reductive elimination (TS2 and TS4) for the analogous 18-electron Fe-PDI metallocycle (i.e. spin cross-over from the restricted singlet manifold to a lower energy triplet), but they found the probability of spin crossover $\langle T_1|\widehat{H}_{SO}|S_0\rangle$ was too low to be an efficient process.[29] It has also been shown experimentally that reductive elimination is substrate induced, meaning that the 16-electron species INT2 and INT4 resulting from this transformation, although stationary points, exist in near zero population due to the small barrier for the reverse reaction, and that complexation of an incoming butadiene monomer is necessary to drive the reaction forward.[28,30] Prior work on Fe-PDI-mediated [2+2] addition of two olefins found that oxidative cyclization proceeded along a 16-electron S=1 manifold ([(PDI^{1-})Fe(I)]→ ([(PDI^{1-})Fe(III)].[31,32] For the transformation studied in this work we do not have any evidence for or against oxidative cyclization proceeding along a similar manifold.

Comparisons between the relative spin energetics at stationary points with known restricted spin states do show UKS and BS manifolds with lower, often substantially, lower energies. The inclusion of exact exchange within the DFT functional lowers the energy of unpaired spin states (e.g. triplet), and as is well documented for hybrid functionals, this addition of exact exchange often incorrectly orders the energetics of the spin states, biasing it towards higher multiplicities.[33,34]

In summary, although we cannot conclusively say for each stationary point which spin state or states are present along the reaction channel, we can say that there is no evidence, to date, which is contrary to a restricted reaction channel.

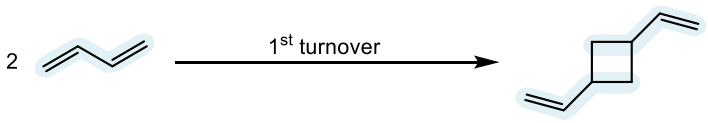

$\Delta(E+ZPE)_r$ or $\Delta G_r = E_{divinylcyclobutane} - 2E_{butadiene}$

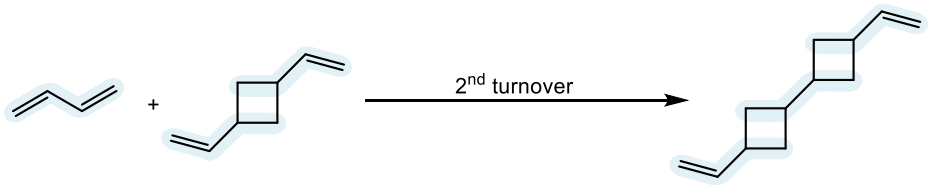

$\Delta(E+ZPE)_r$ or $\Delta G_r = E_{2\text{-}mer} - (E_{butadiene} + E_{divinylcyclobutane})$

Estimation of Reaction Energetics from Organic Components: The reaction energy for the oligomerization of butadiene can also be estimated from the relative change in energy (SCFE+ZPE or G) between the products and the reactants. For the 1st turnover, this would be the energy difference between divinylcyclobutane and two butadienes. For the 2nd turnover, it would be the difference between 1,2'-divinyloligocyclobutane (2-mer) and divinylcyclobutane plus butadiene. In that we are making a near 50/50 mixture of stereoisomers (syn and anti), compounded with the errors in DFT and the rigid-rotor harmonic approximation, we report reaction energies as statistical averages and standard deviations with equal weight given for each stereoisomer (Table 9).

Table 9. Average and standard deviation of changes in reaction energies (E+ZPE) and G at 50 °C and 1 atm in kcal/mol for 1st (syn and anti divinylcyclobutane) and 2nd turnovers (syn-syn, syn-anti, anti-syn, and anti-anti divinyl-2-mer stereoisomers) with respect to butadiene (1st turnover) or divinylcyclobutane (2nd turnover).

	$\Delta(E+ZPE)_r$				**ΔG_r**			
Turnover	First		Second		First		Second	
	mean	s.d.	mean	s.d.	mean	s.d.	mean	s.d.
TPSSh/LACV3P**+//LACVP**	-7.8	0.9	-8.7	2.0	6.6	0.9	5.1	1.5
TPSSh/CPCM/LACV3P**+//LACVP**	-6.2	1.0	-7.4	1.6	8.2	0.9	6.4	1.9
TPSSh/SM8/LACV3P**+//LACVP**	-7.7	0.9	-8.2	1.9	6.7	0.9	5.6	1.6
B3LYP-D3/LACV3P**+//LACVP**	-5.8	0.8	-7.6	1.9	8.7	0.7	6.4	1.7
B3LYP-D3/CPCM/LACV3P**+//LACVP**	-4.2	0.8	-6.2	1.4	10.2	0.8	7.7	2.1
B3LYP-D3/SM8/LACV3P**+//LACVP**	-5.6	0.8	-7.0	1.7	8.9	0.7	6.9	1.8
M06-L/LACV3P**+//LACVP**	-9.0	1.0	-12.1	4.3	5.9	1.7	0.9	0.8
M06-L/CPCM/LACV3P**+//LACVP**	-7.7	1.0	-11.0	3.9	7.2	1.7	2.0	0.5
M06-L/SM8/LACV3P**+//LACVP**	-9.3	1.0	-11.9	4.2	5.6	1.7	1.1	0.7

X. References

1. Schrödinger Release 2019-4**:** Jaguar, Schrödinger, LLC, New York, NY (2019)

2. Bochevarov, A. D. *et al.* Jaguar: a high-performance quantum chemistry software program with strengths in life and materials science. *Int. J. Quantum Chem.* **113**, 2110-2142 (2013).

3. Becke, A. D. Density-functional exchange-energy approximation with correct asymptotic behavior. *Phys. Rev. A* **38**, 3098-3100 (1988).

4. Vosko, S. H. Wilk, L., Nusair, M. Accurate spin-dependent electron liquid correlation energies for local spin density calculations: a critical analysis. *Can. J. Phys.* **58**, 1200-1211 (1980).

5. Lee, C., Yang, W., & Parr, R. G. Development of the Colle-Salvetti correlation-energy formula into a functional of the electron density. *Phys. Rev. B* **37**, 785-789 (1988).

6. Miehlich, B., Savin, A., Stoll, H., Preuss, H. Results obtained with the correlation energy density functionals of Becke and Lee, Yang and Parr. *Chem. Phys. Lett.* **157**, 200-206 (1989).

7. Grimme, S., Antony, J., Ehrlich, S., & Krieg, H. A consistent and accurate *ab initio* parameterization of density functional dispersion correction (DFT-D) for the 94 element H-Pu. *J. Chem. Phys.* **132**, 154104 (2010).

8. Goerigk, L., Grimme, S. A thorough benchmark of density functional methods for general main group thermochemistry, kinetics, and noncovalent interactions. *Phys. Chem. Chem. Phys.* **13**, 6670-6680 (2010).

9. BioVia Materials Studio 2017-R2: Dassault Systèmes, (2016).

10. Jorgensen, W. L., & Tirado-Rives, J. The OPLS [optimized potentials for liquid simulations] potential functions for proteins, energy minimizations for crystals of cyclic peptides and crambin. *J. Am. Chem. Soc.* **110**, 1657-1666 (1988).

11. Jorgensen, W. L., Maxwell, D. S., & Tirado-Rives, J. Development and testing of the OPLS all-atom force field on conformational energetics and properties of organic liquids. *J. Am. Chem. Soc.* **118**, 11225-11236 (1996).

12. Harder, E. *et al*. OPLS3: A force field providing broad coverage of drug-like small molecules and proteins. *J. Chem. Theory Comput.* **12**, 281-296 (2015).

13. Akkermans, R. L. C., Spenley, N. A., & Robertson, S. H. Monte Carlo methods in materials studio. *Molecular Simulation* **39**, 1153-1164 (2013).

14. Sun, H. COMPASS: An *ab initio* forcefield optimized for condensed-phase applications – overview with details on alkane and benzene compounds. *J. Phys. Chem. B.* **102**, 7338-7364 (1998).

15. Sun, H. *et al.* COMPASSII: extended coverage for polymer and drug-like molecule databases. *J. Mol. Model.* **22**, 1-10 (2016).

16. Plimpton, S. Fast parallel algorithms for short-range molecular dynamics, *J. Comp. Phys*. **117**, 1-19 (1995).

17. Materials and Processes Simulations (MAPS version 4.3.0): Scienomics SARL (2004-2019)

18. Schrödinger Release 2019-4**:** MacroModel, Schrödinger, LLC, New York, NY (2019)

19. Tao, J. M., Perdew, J. P., Staroverov, V. N., & Scuseria, G. E. Climbing the density functional ladder: nonempirical meta-generalized gradient approximation designed for molecules and solids. *Phys. Rev. Lett.*, **91,** 146401 (2003).

20. Staroverov, V. N., Scuseria, G. E., Tao, J. & Perdew, J. P. Comparative assessment of a new nonempirical density functional: molecules and hydrogen-bonded complexes. *J. Chem. Phys.*, **119**, 12129 (2003). [Erratum] **121**, 11507(E) (2003).

21. Cirera, J., Via-Nadal, M., & Ruiz, E. Benchmarking density functional methods for calculation of state energies of first row spin-crossover molecules. *Inorg. Chem.* **57**, 14097-14105 (2018).

22. Hay, J. P., & Wadt, W. R. Ab initio effective core potentials for molecular calculations. Potentials for K to Au including the outermost core orbitals. *J. Chem. Phys.* **82**, 299-310 (1985).

23. Cossi, M., Rega, N., Scalmani, G., & Barone, V. Energies, structures, and electronic properties of molecules in solution with the C-PCM solvation model. *J. Comp. Chem.*, **24**, 669-681 (2003).

24. Marenich, A. V., Olson, R. M., Kelly, C. P., Cramer, C. J., & Truhlar, D. G. Self-consistent reaction field model for aqueous and nonaqueous solutions based on accurate polarized partial charges, *J. Chem. Theory Comput.* **3**, 2011-2033 (2007).

25. Kozuch, S., & Shaik, S. How to conceptualize catalytic cycles? The energetic span model. *Acc. Chem. Res.* **44**, 101-110 (2011).

26. S. T. Soda, Y. Kitagawa, T. Onishi, Y. Takano, Y. Shigeta, H. Nagao, Y. Yoshioka, K. Yamaguchi. Ab initio computations of effective exchange integrals for H–H, H–He–H and Mn_2O_2 complex: comparison of broken-symmetry approaches. *Chem. Phys. Lett.* **319**, 223-230 (2000).

27. F. Neese. Prediction of Molecular Properties and Molecular Spectroscopy with Density Functional Theory: From Fundamental Theory to Exchange-Coupling. *Coord. Chem. Rev.* **253**, 526-563 (2009).

28. S. K. Russell, E. Lobkovsky, P. J. Chirik. Iron-Catalyzed Intermolecular [2π+2π] Cycloaddition. *J. Am. Chem. Soc.* **133**, 8858-8861 (2011).

29. L. Hu, H. Chen. Substrate-Dependent Two-State Reactivity in Iron-Catalyzed Alkene [2+2] Cycloaddition Reactions. *J. Am. Chem. Soc.* **139**, 15564-15567 (2017).

30. J. M. Hoyt, V. A. Schmidt, A. M. Tondreau, P. J. Chirik. Iron-Catalyzed Intermolecular [2+2] Cycloadditions of Unactivated Alkanes. *Science* **349**, 960-963 (2015).

31. J. M. Hoyt, K. T. Sylvester, S. P. Semproni, P. J. Chirik. Synthesis and Electronic Structure of Bis(imino)pyridine Iron Metallacylic Intermediates in Iron-Catalyzed Cyclization Reactions. *J. Am. Chem. Soc.* **135**, 4862-4877 (2013)

32. M. V. Joannou, J. M. Hoyt, P. J. Chirik. Investigations into the Mechanism of Inter- and Intramolecular Iron-Catalyzed [2+2] Cycloaddition of Alkenes. *J. Am. Chem. Soc.* **142**, 5314-5330 (2020).

33. S. Ye, F. Neese. Accurate Modeling of Spin-State Energetics in Spin-Crossover Systems with Modern Density Functional Theory. *Inorg. Chem.* **49**, 772-774 (2010).

34. J. M. Darmon, S. C. E. Stieber, K. T. Sylvester, I. Fernandez, E. Lobkovsky, S. P. Semproni, E. Bill, K. Wieghardt, S. DeBeer, P. J. Chirik. Oxidative Addition of Carbon-Carbon Bonds with a Redox-Active Bis(imino)pyridine Iron Complex. *J. Am. Chem. Soc.* **134**, 17125-17137 (2012).